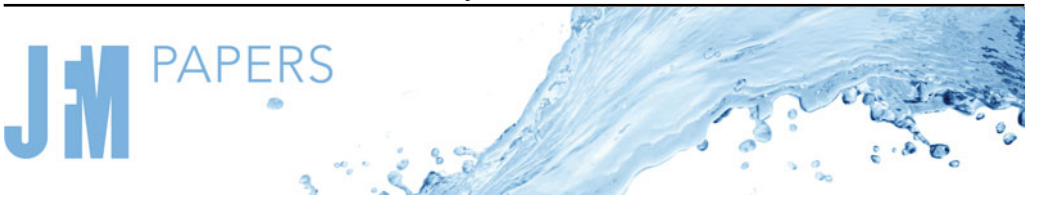
J. Fluid Mech. (2025), *vol.* 1015, A22, doi:10.1017/jfm.2025.10268



Interactions of flexural-gravity and interfacial waves in a two-layer fluid with a discontinuous background mean flow

Susam Boral[1,2], **Bao-Yu Ni**[1] and **Alexander A. Korobkin**[3]

[1]College of Shipbuilding Engineering, Harbin Engineering University, Harbin, PR China

[2]Department of Civil, Structural and Environmental Engineering, Trinity College Dublin, Dublin, Ireland

[3]School of Mathematics, University of East Anglia, Norwich, UK

Corresponding author: Susam Boral, susamboral@gmail.com

(Received 8 October 2024; revised 18 April 2025; accepted 16 May 2025)

This study investigates the interactions between flexural-gravity waves and interfacial waves in a two-layer fluid, focusing on wave blocking. Both liquid layers are of finite depth bounded on top by a viscoelastic thin plate. Both liquids are incompressible and inviscid, and their flows are two-dimensional and potential. Linear wave theory and a linear equation of a thin floating viscoelastic plate of constant thickness are used. We analyse the phenomenon of wave blocking and Kelvin–Helmholtz (KH) instability in a two-layer fluid with a discontinuous background mean flow. A quartic dispersion relation for frequency as a function of wavenumber and other parameters of the problem is derived. Two cases of uniform current and layers moving with different velocities are studied. Wave blocking occurs when roots of the dispersion relation coalesce without accounting for plate viscosity, leading to zero group velocity. Our findings indicate that wave blocking can occur for both flexural-gravity and interfacial waves under various frequency and current speed conditions, provided that plate viscosity is absent. The role of different parameters and the flow velocities of the upper and lower layers are investigated in the occurrence of wave blocking and KH instability. The loci of the roots of the dispersion relation involving plate viscosity depict that no root coalescence occurs irrespective of the values of wavenumber and frequency in the presence of plate viscosity. The amplitude ratio of the interfacial wave elevation to that of floating viscoelastic plate deflection exhibits the dead-water phenomenon as a density ratio approaches unity.

Key words: ice sheets, internal waves, stratified flows

© The Author(s), 2025. Published by Cambridge University Press.

https://doi.org/10.1017/jfm.2025.10268 Published online by Cambridge University Press

1. Introduction

Over the decades, there has been a renewed interest in studying flexural-gravity waves generated by the interaction of surface gravity waves with floating elastic plates or ice sheets. The need for transport and field operations on ice in polar regions drives this interest. A practical example of this can be seen in Antarctica, where helicopters ('HeloOps') have been used to transport supplies by landing directly on the ice surface at McMurdo Sound (see Fox 2011). A parallel branch of study focuses on the interaction of waves with floating flexible structures, which is crucial for the utilisation of ocean space in constructing floating bridges, runways, storage facilities and other floating structures. Lamas-Pardo, Iglesias & Carral (2015) conducted a comprehensive review to provide insights into the potential benefits and challenges of using very large floating structures (VLFSs) in various coastal and offshore applications. Squire (2020) established a synergy between the wave–ice interaction and the wave interaction with floating structures, as floating ice sheets and VLFSs are often modelled as thin elastic plates in both areas of study. Ocean currents profoundly influence the propagation of flexural-gravity waves in homogeneous and stratified fluids. Complexity arises in the presence of a shear current across the interface in a stratified ocean. To better understand this wave dynamics, this study employs a linear hydroelastic model of a two-layer density-stratified fluid with relative motion between the layers in finite water depths.

In coastal environments, as well as in polar regions where human activities and infrastructures are concentrated, the study of plane flexural-gravity waves is crucial when the floating elastic plate or ice sheet is subjected to external vibrating loads. These plane waves are predominant on the plate-covered surface away from the excitation point. The external stationary and vibrating loads on floating flexible plates are characterised by a combination of steady and oscillatory forces exerted by environmental factors and human activities (Matiushina, Pogorelova & Kozin 2016). These loads result in complex stress and deformation patterns, requiring careful analysis of wave characteristics for structural integrity and stability of sea ice or floating structures. In the study of wave–ice interaction, flexural-gravity waves are important. They are analysed by the linear theory of hydroelasticity (see Greenhill 1886; Zeng *et al.* 2021). Flexural-gravity wave patterns on an ice sheet caused by a moving load with uniform speed were described by Kheisin (1963) and Davys, Hosking & Sneyd (1985). In a subsequent study, Schulkes, Hosking & Sneyd (1987) introduced additional modelling features like a structural compressive force and current under the ice in investigating the response of floating ice to a steadily moving source. They demonstrated that a uniform flow beneath the ice re-oriented the flexural-gravity wave pattern in the direction of the load velocity. Peake (2001) investigated the nonlinear evolution of negative-energy waves and convective instabilities in floating elastic plate–mean flow interactions along with solitary-wave behaviour under specific conditions, governed by the nonlinear Schrödinger equation. Later, Peake (2004) analysed the dynamic behaviour of fluid-loaded elastic plates in uniform mean flow, demonstrating the emergence of instabilities such as negative-energy waves, resonant solutions and nonlinear fluttering due to pre-tension, spring foundations and structural damping. The book by Nevel (1970) and the monograph by Squire *et al.* (2012) summarised the theory and various field experiments on wave–ice interaction, offering scientists and practitioners a comprehensive resource on ice response to moving loads, which often differs significantly from the response to stationary loads. Recently, Tkacheva (2024) studied the response of floating ice to the uniform rectilinear motion of a time-independent load in the presence of a shear current. These studies mentioned the importance of understanding the plane flexural-gravity wave characteristics in order to examine the

https://doi.org/10.1017/jfm.2025.10268 Published online by Cambridge University Press

plate response to an external load. This study analyses the behaviour of flexural-gravity waves propagating in the following and opposing directions of the current in complex oceanographic settings.

In the present study, a viscoelastic model of ice sheets and floating flexible structures is used. The Kelvi–Voigt model of viscoelastic plates is used due to its simplicity, reasonable accuracy and high explanatory ability. This model is well suited for capturing ice deformation under the action of the load on a floating ice sheet. Tabata (1958) performed experiments with rectangular ice beams under stationary loads and obtained stress–time curves. He concluded that the viscoelastic properties of sea ice can be well described by a rheological model consisting of a Maxwell unit and a Kelvin–Voigt unit connected in series with four characteristic constants. Takizawa (1985) conducted experiments to measure the deflections of an ice sheet caused by a moving vehicle. He revealed that the maximum deflection of the ice sheet lagged behind the vehicle, even at relatively low speeds of the vessels. Further, his study showed that the maximum deflection caused by a moving load was three times greater than that caused by an equivalent static load. Hosking, Sneyd & Waugh (1988) used two-parameter viscoelastic models involving Kelvin–Voigt and Maxwell units for theoretical predictions of ice responses to moving loads. Kozin & Pogorelova (2009) used the Kelvin–Voigt, Maxwell and generalised Maxwell–Kelvin models to describe the viscoelastic characteristics of ice, comparing their theoretical predictions with Takizawa's (1985) experimental results. They concluded that, for accurate predictions, the retardation time, representing the viscosity of ice, should vary with the load speed in these models. Shishmarev, Khabakhpasheva & Korobkin (2016) studied the deflections and stresses in a viscoelastic ice cover of a frozen channel induced by a load moving at a constant speed along the channel. Zeng *et al.* (2022) investigated the deflection of a floating viscoelastic ice sheet with a line crack due to a localised moving load. Khabakhpasheva & Korobkin (2021) studied the vertical impact of a rigid blunt body on a floating viscoelastic ice floe. Recently, Tavakoli & Babanin (2023) used two-parameter viscoelastic solid models incorporating Kelvin–Voigt (KV) and Maxwell mechanisms, along with a one-parameter elastic solid model, to describe the rheological behaviour of the ice layer. Recently, Boral & Ni (2025) studied the response of a floating viscoelastic plate to a time-periodic and moving external load in a homogeneous fluid.

Apart from considering a homogeneous fluid beneath the floating plate, the present study deals with a two-layer density-stratified fluid with the upper layer sitting on top of the denser lower layer. Density stratifications in fluids can be caused by changes in temperature or salinity across water depth in the case of the ocean (see Bebieva & Timmermans 2019, and references therein). Stokes (1847) first explained the existence of both surface and internal waves in a two-layer density-stratified fluid. In the early twenty-first century, Alam *et al.* (2009*a*,*b*) conducted significant theoretical and numerical studies on the nonlinear interactions of surface-interfacial waves in the presence of a bottom ripple, highlighting the occurrence of the Bragg resonance phenomenon. Building upon this foundation, the present study investigates the linear interactions of surface-interfacial waves with discontinuous background mean flows. This research aims to contribute valuable insights that can enhance our understanding of the nonlinear Bragg resonance phenomenon in a two-layer fluid system with a viscoelastic plate-covered surface. Schulkes *et al.* (1987) explained that a load steadily moving along floating ice excites an interfacial wave in a two-layer stratified ocean. Besides, the study explained that, for load speeds greater than a minimum phase speed, both flexural-gravity and interfacial waves are generated. However, slower loads induced only interfacial waves. Duffy (1996) generalised the study of Schulkes *et al.* (1987) to a vibrating line load moving along a thin elastic ice floating on a two-layer density-stratified fluid. This study explained that the longer wavelength of

https://doi.org/10.1017/jfm.2025.10268 Published online by Cambridge University Press

the ice response results in a shorter interfacial wave with a larger amplitude. Czipott *et al.* (1991) measured ice flexure induced by internal wave packets near the Yermak Plateau, and the study revealed significant tilt, strain and displacement effects, highlighting interactions between Arctic ice and the subsurface dynamics. Sturova (2011) analysed the dynamics of floating ice influenced by the steady oscillations of a submerged cylinder in a stratified fluid. Another interesting aspect of a two-layer fluid is the dead-water phenomenon, known to sailors since ancient times, which elucidates the abnormal resistance experienced by ships in visibly still water. Ekman (1904) provided the first scientific explanation, attributing the increased ship resistance to the generation of interfacial waves. His study is further developed by Tulin & Zilman (1993) in a linear context and Grue, Bourgault & Galbraith (2016) in a nonlinear framework. Wang *et al.* (2014) studied steady solitary and generalised solitary waves in a two-fluid system under an elastic sheet, modelling internal waves beneath ice-covered oceans. Using a fully nonlinear thin shell model and boundary integral methods, they demonstrated distinct behaviours of barotropic and baroclinic modes, including wave-packet solitary waves and new Wilton-ripple-like patterns in generalised solitary waves, highlighting the impact of elasticity on the wave dynamics. Părău (2018) studied solitary waves along an elastic plate between two fluids of differing densities in the cases of a rigid lid-covered surface and a floating elastic plate; the study derived dispersion relations and computed the nonlinear solutions numerically. Das *et al.* (2018*c*) studied the dead-water analogue of flexural-gravity waves in a two-layer fluid and explained a significant growth in interfacial wave amplitude when the variations in densities across the layers are small. In a different context, Boral *et al.* (2022) analysed the dead-water analogue of capillary-gravity waves in a two-layer fluid system with surface and interfacial tensions, and currents in the layers. The pioneering simulation-based study by Hao & Shen (2020) successfully captured the surface roughness signature induced by internal solitary waves in oceans using a deterministic two-layer model, effectively overcoming the singularity issues associated with traditional wave–current interaction theory. Martin & Părău (2025) developed a Hamiltonian framework for hydroelastic waves in stratified, rotational fluids with ice-covered surfaces provides insights into the wave dynamics with discontinuous stratification and shear currents.

In our study, the presence of a discontinuous mean flow across the interface in a two-layer fluid leads to wave blocking in the case of counter-propagating waves for a given frequency. Wave blocking occurs when the wave energy transport velocity vanishes. This complex phenomenon is not yet fully understood. In the work of Duffy (1991, 1996), this phenomenon of vanishing wave energy transport velocity is termed resonance. Wave blocking occurs when waves generated by a static load encounter opposing currents, which significantly reduce the group speed of the waves. Smith (1975) proposed a uniform asymptotic solution for surface gravity waves on a collinear, adverse and slowly varying current. Instead of wave breaking, in which the wave amplitude reaches the point where the crest of the wave overturns, their solution demonstrated wave reflection near the blocking region. It is worth mentioning that, when gravity waves interact with opposing currents, their wavelengths shorten, and wave reflection takes place when blocking occurs. Trulsen & Mei (1993) examined the transformation of capillary-gravity waves by opposing current in the blocking region. Various experiments were performed to validate the theory of wave blocking (Ris & Holthuijsen 1996; Chawla & Kirby 1999, 2002). Maïssa *et al.* (2016) studied the dispersion properties of surface waves with surface tension and investigated the blocking phenomenon for shear flows gradually varying in a horizontal direction. Apart from analysing wave blocking, the occurrence of Kelvin–Helmholtz instability is studied using the potential flow theory in the presence of a relative motion

https://doi.org/10.1017/jfm.2025.10268 Published online by Cambridge University Press

between the fluid layers in finite water depth, (see Cairns 1979; Bontozoglou & Hanratty 1988; Fabrikant & Stepanyants 1998).

In the last decade, the wave blocking in the system of compressed elastic plates floating on the surface of either homogeneous or two-layer fluid was intensively investigated (Negi, Boral & Sahoo 2022; Barman, Boral & Sahoo 2023; Bisht *et al.* 2023; Boral *et al.* 2023*a*,*b*). The present study distinguishes itself from the work by Das *et al.* (2018*c*), which focused on wave blocking involving a thin elastic plate and included plate compression but did not explore the relative motion between the upper and lower layers, and plate viscosity. Here, we extensively study the relative motion effects in conjunction with the interactions between flexural-gravity and interfacial waves in finite water depth. It is pertinent to note that Boral *et al.* (2022) focused on deriving the dispersion relation for capillary-gravity waves in a two-layer density-stratified fluid with a tangential discontinuity of velocity at the interface. The analysis primarily examined wave blocking under the assumptions of uniform current and a moving upper layer over a stationary lower layer for short capillary-gravity waves. Boral *et al.* (2021*a*) studied flexural-gravity wave blocking by incorporating the effects of elastic and viscoelastic foundations in an infinitely extended floating elastic plate. The study concluded that no wave blocking occurs when the floating elastic plate is supported on a viscoelastic foundation. In the linear approximation, Stepanyants & Sturova (2021) analysed the wave motions of a compressed elastic ice sheet induced by a two-dimensional dipole moving in the water beneath the ice sheet within the context of wave blocking. Das *et al.* (2018*a*) investigated flexural-gravity wave propagation under compressive forces and flow vorticity using linear water wave theory, demonstrating phenomena such as wave blocking.

The novelty of the present study is to deeply investigate the interactions of flexural-gravity waves with an interfacial wave in a two-layer fluid moving with different speeds within the paradigm of wave blocking. The KV model is used for structural analysis to incorporate viscous damping. The paper is organised as follows: in § 2, the two-dimensional mathematical model is formulated under the assumption that the upper and lower layers are moving at different uniform speeds. Section 3 derives a complicated dispersion relation for flexural-gravity waves in a two-layer fluid with a plate-covered surface and free interface, along with the different uniform currents in each layer. The dispersion relation gives no real wavenumber in the presence of plate viscosity. In § 4, the independent short flexural-gravity and interfacial waves are analysed to determine the criteria for the occurrence of wave blocking. Additionally, the criteria for the occurrence of Kelvin–Helmholtz instability in the short interfacial wave is derived. Section 5 demonstrates the role of relative motion between the layers in the occurrences of wave blocking in flexural-gravity and interfacial waves when there is an interaction between them in finite water depth. It is observed that wave blocking does not occur simultaneously in flexural-gravity and interfacial waves under any conditions. Additionally, multiple wave interactions are possible either on the plate-covered surface or on the interface for certain values of current and wave frequency. Section 6 depicts that wave blocking disappears in the presence of plate viscosity. However, the interactions of multiple waves on the plate-covered surface or the interface are possible under certain conditions. It is found that the flexural-gravity and the interfacial waves decay rapidly for higher values of plate viscosity. In § 7 the phenomenon of the dead-water analogue of flexural-gravity waves in a two-layer fluid with current is investigated with account for structural damping. It is pertinent to note that the analysis of this paper is performed in dimensional variables. Dimensionless variables and analysis using them are standard in theoretical studies but less common in physical and engineering research (Dingemans 1997; Squire *et al.* 2012). However, where it is helpful, the obtained results are presented in dimensionless variables, making

https://doi.org/10.1017/jfm.2025.10268 Published online by Cambridge University Press

the results applicable to other cases. Key findings and conclusions of this study are summarised in § 8.

2. Formulation of the problem

Linear waves propagating in a two-layer density-stratified fluid with a free interface and a viscoelastic plate floating on the surface of the upper layer are studied. Viscous properties of the floating plate are described using the KV model with retardation time τ. The flow is considered in the Cartesian coordinate system, Oxy, where the line $y = 0$ corresponds to the plate/liquid interface, the line $y = -h$ corresponds to the equilibrium position of the free interface between the layers and the line $y = -H$ corresponds to the bottom of the lower liquid layer. The upper layer is of depth h and density ρ_1. The lower layer is depth $H-h$ and density ρ_2. The density ratio $s = \rho_1/\rho_2$ is less than one for the stability of the two-layer liquid. The ambient velocities of the flow in the upper and lower layers are U_1 and U_2, respectively. The fluids in the layers are inviscid and incompressible, with their flows being two-dimensional and potential.

The velocity potentials in the layers are $\Phi_j^U(x, y, t) = U_j x + \Phi_j(x, y, t)$, where $j = 1$ is for the upper layer and $j = 2$ is for the lower layer. Within the linear wave theory, the potentials $\Phi_j(x, y, t)$ satisfy the Laplace equations in the corresponding layers

$$\nabla^2 \Phi_j = 0 \qquad -\infty < x < \infty \text{ and } \begin{cases} -h < y < 0 & \text{for } j = 1, \\ -H < y < -h & \text{for } j = 2, \end{cases} \tag{2.1}$$

the bottom boundary condition

$$\frac{\partial \Phi_2}{\partial y} = 0 \qquad \text{on } y = -H, \tag{2.2}$$

the linearised kinematic boundary condition on the plate/liquid interface

$$\frac{\partial \Phi_1}{\partial y} = \left(\frac{\partial}{\partial t} + U_1 \frac{\partial}{\partial x}\right) \eta_1 \qquad \text{on } y = 0, \tag{2.3}$$

where $\eta_1(x, t)$ is the deflection of the viscoelastic plate, $y = \eta_1(x, t)$, and the linearised kinematic boundary conditions on the free interface

$$\left(\frac{\partial}{\partial t} + U_1 \frac{\partial}{\partial x}\right) \eta_2 = \frac{\partial \Phi_1}{\partial y}, \tag{2.4}$$

$$\left(\frac{\partial}{\partial t} + U_2 \frac{\partial}{\partial x}\right) \eta_2 = \frac{\partial \Phi_2}{\partial y} \qquad \text{on } y = -h, \tag{2.5}$$

where the interface shape is described by the equation $y = -h + \eta_2(x, t)$ and the function $\eta_2(x, t)$ represents the free interface elevation. Conditions (2.4) and (2.5) imply the continuity of normal velocity across the interface

$$\frac{\partial \Phi_1}{\partial y} - \frac{\partial \Phi_2}{\partial y} = (U_1 - U_2) \frac{\partial \eta_2}{\partial x} \qquad \text{on } y = -h. \tag{2.6}$$

Here, we adopt a refined formulation of the equation of continuity at the interface to accommodate the motion of upper and lower layers moving at different speeds, improving upon the approach taken in Boral *et al.* (2022).

https://doi.org/10.1017/jfm.2025.10268 Published online by Cambridge University Press

The thin viscoelastic plate is governed by the equation (see Squire *et al.* 2012; Lakes 2017)

$$\left[EI\left(1+\tau\frac{\partial}{\partial t}\right)\frac{\partial^4}{\partial x^4}+M\frac{\partial^2}{\partial t^2}\right]\eta_1 = p_H(x,0,t) \quad \text{on } y=0, \tag{2.7}$$

where E is the Young's modulus of the plate material, $I = d^3/\{12(1-\nu^2)\}$ is the moment of inertia of the plate, d and ν are the plate thickness and Poisson's ratio respectively, $M = \rho_p d$ is the mass of the plate per unit area, ρ_p is the plate density and $p_H(x,0,t)$ is the hydrodynamic pressure on the plate/liquid interface. The hydrodynamic pressure, $p_H(x,0,t)$, is given by the linearised Bernoulli equation. On the plate/liquid interface $y=0$

$$p_H(x,0,t) = -\rho_1\left\{\left(\frac{\partial}{\partial t}+U_1\frac{\partial}{\partial x}\right)\Phi_1(x,0,t)+g\eta_1(x,t)\right\}. \tag{2.8}$$

Equations (2.8) and (2.7) yield

$$\left[EI\left(1+\tau\frac{\partial}{\partial t}\right)\frac{\partial^4}{\partial x^4}+M\frac{\partial^2}{\partial t^2}+\rho_1 g\right]\eta_1 = -\rho_1\left(\frac{\partial}{\partial t}+U_1\frac{\partial}{\partial x}\right)\Phi_1(x,0,t) \quad \text{on } y=0. \tag{2.9}$$

Eliminating η_1 from (2.9) using (2.3), the following boundary condition for the potential $\Phi_1(x,y,t)$ is derived

$$\left[EI\left(1+\tau\frac{\partial}{\partial t}\right)\frac{\partial^4}{\partial x^4}+M\frac{\partial^2}{\partial t^2}+\rho_1 g\right]\frac{\partial\Phi_1}{\partial y} = -\rho_1\left(\frac{\partial}{\partial t}+U_1\frac{\partial}{\partial x}\right)^2\Phi_1 \quad \text{on } y=0. \tag{2.10}$$

The continuity of the hydrodynamic pressure, see (2.8), at the interface $y=-h$, provides the linearised dynamic free interface boundary condition in terms of the potentials $\Phi_1(x,y,t)$ and $\Phi_2(x,y,t)$

$$s\left\{\left(\frac{\partial}{\partial t}+U_1\frac{\partial}{\partial x}\right)\Phi_1+g\eta_2\right\} = \left(\frac{\partial}{\partial t}+U_2\frac{\partial}{\partial x}\right)\Phi_2+g\eta_2 \qquad \text{on } y=-h, \tag{2.11}$$

with $s=\rho_1/\rho_2$ being the density ratio, $0<s<1$.

3. Plane wave solutions

In this section, the plane wave solutions associated with flexural-gravity waves on the viscoelastic plate-covered surface and interfacial waves on the interface in a two-layer fluid are studied. The linear waves propagating on the two-layer fluids are sought in the form

$$\eta_j(x,t) = \mathrm{Re}\left\{\eta_{j0}\mathrm{e}^{\mathrm{i}(px-\Omega t)}\right\}, \qquad \text{for } j=1,2, \tag{3.1}$$

where η_{10} and η_{20} are complex amplitudes of the plate deflection and free interface elevation, respectively, p is the wavenumber and Ω is the angular frequency. Using (2.1)–(2.3), the velocity potentials $\Phi_j(x,y,t)$ associated with the waves (3.1) can be written in the forms

$$\Phi_1(x,y,t) = \mathrm{Re}\left\{(A\cosh(py)+B\sinh(py))\mathrm{e}^{\mathrm{i}(px-\Omega t)}\right\}, \tag{3.2}$$

$$\Phi_2(x,y,t) = \mathrm{Re}\left\{C\cosh\{p(y+H)\}\mathrm{e}^{\mathrm{i}(px-\Omega t)}\right\}, \tag{3.3}$$

https://doi.org/10.1017/jfm.2025.10268 Published online by Cambridge University Press

where A, B and C are the complex coefficients to be determined. Note that we are working on the dimensional variables.

Using (2.3), (2.5) and (2.11), the complex coefficients A, B and C are obtained as

$$A = \mathrm{i}\left\{g(1-s) - \frac{\Omega_{r2}^2}{p}\coth\{p(H-h)\}\right\}\frac{\eta_{20}}{s\cosh(ph)\Omega_{r1}} - \frac{\mathrm{i}\Omega_{r1}\eta_{10}}{p\coth(ph)}, \tag{3.4}$$

$$B = -\frac{\mathrm{i}\Omega_{r1}}{p}\eta_{10}, \tag{3.5}$$

$$C = -\frac{\mathrm{i}\Omega_{r2}}{p\sinh\{p(H-h)\}}\eta_{20}, \tag{3.6}$$

where $\Omega_{rj} = \Omega - pU_j$ are the Doppler-shifted frequencies in the upper and lower layers for $j = 1$ and $j = 2$, respectively. Equation (2.6) provides the amplitude ratio of the free interface elevation η_{20} to that of plate deflection η_{10}

$$\frac{\eta_{20}}{\eta_{10}} = \frac{s\Omega_{r1}^2}{\sinh(ph)\left[\Omega_{r2}^2 C_{H-h} + s\Omega_{r1}\Omega_{r2}C_h - g(1-s)p + sp\Delta U C_h \Omega_{r1}\right]}, \tag{3.7}$$

where $C_h = \coth(ph)$, $C_{H-h} = \coth\{p(H-h)\}$ and $\Delta U = U_2 - U_1$. In the limit $s \to 0$, where the lower liquid is much heavier than the upper one, (3.7) predicts that the interface can be treated as a rigid boundary with $\eta_{20} = 0$. For large values of the ratio (3.7), the amplitude of the interfacial waves is much greater than that of the flexural-gravity wave. We are concerned with the effects of the current velocities U_1 and U_2, as well as the retardation time τ, on the characteristics of the flexural-gravity waves and the interfacial waves propagating along the interfaces $y = 0$ and $y = -h$ respectively. We are also concerned with the interactions of these waves, which are affected by the current.

Substituting (3.2) in (2.10) and using (3.4), (3.5) and (3.7), the following dispersion relation for waves in a two-layer fluid with a tangential discontinuity of velocity is obtained

$$\{\rho_1\Omega_{r1} + \rho_2 C_h C_{H-h}\Omega_{r2}\}\rho_1\Omega_{r1}^2\Omega_{r2} + \{\rho_1\Delta U\Omega_{r1} - (\rho_2 - \rho_1)gC_h\}\rho_1 p\Omega_{r1}^2 + \mathcal{A}\mathcal{D}_{r1,r2} = (\mathrm{i}\tau\Omega)EIp^4\mathcal{D}_{r_1,r_2}, \tag{3.8}$$

where

$$\begin{aligned}\mathcal{A} &= EIp^4 + \rho_1 g - M\Omega^2,\\ \mathcal{D}_{r1,r2} &= -\rho_2\mathcal{B}_{r_1,r_2} - \rho_1\Delta U p^2 C_h\Omega_{r1},\\ \mathcal{B}_{r_1,r_2} &= spC_h\Omega_{r1}\Omega_{r2} + pC_{H-h}\Omega_{r2}^2 - (1-s)gp^2.\end{aligned} \tag{3.9}$$

The dispersion relation (3.8) is a quartic equation with respect to the frequency Ω as a function of the wavenumber p and parameters of the system. There are four complex roots of this equation for any real p, from $-\infty$ to ∞ in the presence of τ. On the contrary, the roots Ω become real for complex p with $\tau > 0$, and we are concerned only with real roots Ω. Note that the left-hand side of (3.8) does not change if p is changed to $-p$ and Ω is changed to $-\Omega$. Therefore, the roots of dispersion relation (3.8) are odd functions of the wavenumbers p if $\tau = 0$. For viscoelastic plates with $\tau > 0$, the right-hand side of (3.8) changes its sign if p is replaced by $-p$ and Ω is replaced by $-\Omega$. We conclude that only positive $\Omega\,(\geq 0)$ are enough to consider for elastic plates without viscous properties.

The roots of $\Omega(p)$ of the dispersion relation (3.8) depend on nine dimensional parameters EI, g, ρ_1, ρ_2, U_1, U_2, M, H, h. Introducing dimensionless parameters reduces the number of parameters by two. In any case, it is complicated to describe

https://doi.org/10.1017/jfm.2025.10268 Published online by Cambridge University Press

flexural-gravity waves, interfacial waves and their interaction for such complex systems. To gain a clear insight into the general characteristics of these waves, we start with two special cases of the currents. In both cases, $\tau = 0$ and $M = 0$, which makes $\mathcal{A}$ independent of the frequency Ω.

In the first case, the velocities of the currents in each layer are equal, $U_1 = U_2 = U$. This is the case without velocity discontinuity at the free interface. In this case, the complexity of (3.8) is reduced, allowing clearer insights into the behaviour of the system to be gained without losing physical accuracy. Note that the problem of a load moving along the viscoelastic ice sheet at a speed U in a moving coordinate system can easily be analysed from the present reference case with appropriate modifications to the surface boundary condition (2.10). Consequently, the dispersion relation (3.8) reduces to

$$A_1\Omega_U^4 - A_2\Omega_U^2 + A_3 = (\mathrm{i}\tau)EI\{(1-s)gp^2 - spC_h\Omega_U^2 - pC_{H-h}\Omega_U^2\}p^4\Omega, \tag{3.10}$$

where $\Omega_U = \Omega - pU$ and

$$A_1 = \rho_1(s + C_hC_{H-h}), \tag{3.11}$$

$$A_2 = \rho_1 gp(1-s)C_h + (sC_h + C_{H-h})p\mathcal{A}, \tag{3.12}$$

$$A_3 = (1-s)gp^2\mathcal{A}. \tag{3.13}$$

The dispersion relation (3.10) with $\tau = 0$ and $M = 0$ yields

$$\Omega_{U\pm}^2 = \frac{A_2 \pm \sqrt{A_2^2 - 4A_1A_3}}{2A_1}, \tag{3.14}$$

where the subscripts '+' and '−' are associated with the faster and slower modes, respectively. Note that the coefficients A_j for $j = 1,\ 2$ and 3 are real, positive and even functions of p. The faster and slower modes are referred to as the flexural-gravity wave and interfacial wave, respectively, as shown in Das *et al.* (2018*c*). It can be shown that the faster mode provides the amplitude ratio (3.7) less than one in module. Therefore, the faster mode with '+' in (3.14) has an amplitude that is higher at the plate/liquid interface than at the free interface. On the contrary, the slower mode provides the module with an amplitude ratio higher than one, indicating a mode with a higher amplitude at the free interface between the fluid layers. The waves on the plate-covered surface and on the free interface are also referred to as the barotropic and baroclinic modes, respectively (see Kundu, Cohen & Dowling 2015).

In the second case, we consider the upper layer moving at a certain speed over a stationary lower layer. This is related to flexural-gravity wave propagation in a two-layer density-stratified fluid with a discontinuous mean flow across the interface. Setting $U_1 = U$ and $U_2 = 0$, (3.8) is simplified to

$$\{\rho_1\Omega_{r1} + \rho_2C_hC_{H-h}\Omega\}\,\rho_1\Omega_{r1}^2\Omega + \{\rho_1\Delta U\Omega_{r1} - (\rho_2-\rho_1)gC_h\}\,\rho_1 p\Omega_{r1}^2 + \mathcal{A}\mathcal{D}_{r_1} = (\mathrm{i}\tau\Omega)EIp^4\mathcal{D}_{r_1}, \tag{3.15}$$

where $\mathcal{D}_{r1}$ is equal to $\mathcal{D}_{r1,r2}$, see (3.8), with Ω_{r2} being replaced by Ω. The dispersion relations (3.10) and (3.15) are still complicated for thorough analysis. We will start with reference cases for each of the equations, where each layer is very deep compared with the wavelength of the linear propagating waves, which corresponds to the short waves. In these reference cases, the interfacial waves localised at $y = -h$, and the flexural-gravity waves localised at $y = 0$ are independent, and each (3.10) and (3.15) can be decomposed into two equations for corresponding wave types. Wave blocking and other special cases

https://doi.org/10.1017/jfm.2025.10268 Published online by Cambridge University Press

are analysed in § 4. In § 5, it will be shown how wave characteristics are modified for longer waves with strong interaction between the flexural-gravity and interfacial waves.

4. Deep-water approximation and wave blocking

Deep water, or in other words, short wave approximation with $|p|h \gg 1$ and $|p|(H-) \gg 1$ are applied to the dispersion relation (3.10) and (3.15). We have $C_h \approx p/|p|$ and $C_{H-h} \approx p/|p|$ within this approximation. We consider $\tau = 0$ and $M = 0$ in this section.

4.1. *Uniform current in the upper and lower layers*

The dispersion relation (3.10) for the currents with equal velocities U in each layer provides within the deep-water approximations, $A_1 = \rho_1(1+s)$, $A_2 = \rho_1 g|p|(1-s) + (1+s)|p|\mathcal{A}$, $A_3 = (1-s)gp^2\mathcal{A}$, $\mathcal{A} = EIp^4 + \rho_1 g$ and $\Omega_U = \Omega - pU$. The limiting dispersion relation can be decomposed as

$$A_1\big(\Omega_U^2 - \Omega_{US}^2\big)\big(\Omega_U^2 - \Omega_{UI}^2\big) = 0, \tag{4.1}$$

where

$$\Omega_{US}^2 = \frac{|p|}{\rho_1}\big(EIp^4 + \rho_1 g\big), \tag{4.2}$$

$$\Omega_{UI}^2 = rg|p|, \tag{4.3}$$

and $r = (1-s)/(1+s)$. Equations (4.2) and (4.3) are the dispersion relations of flexural-gravity and internal gravity waves with current within the deep-water approximations, see equation (10) in Mohanty, Mondal & Sahoo (2014), which leads to (4.2) without accounting for both compression in the floating plate and the plate mass.

Equation (4.2) describes flexural-gravity waves for infinitely deep fluid with a current. In the deep-water limit, these waves are independent of the presence of the interface at $y = -h$. Equation (4.2) provides two wave systems

$$\Omega_S^{\pm} = pU \pm \sqrt{\frac{|p|}{\rho_1}\big(EIp^4 + \rho_1 g\big)}. \tag{4.4}$$

Without loss of generality, we take the current velocity U to be negative, which implies that the current goes from right to left, see figure 1. Then $\Omega_S^+ > 0$ for $p < 0$ and the phase velocity $\Omega_S^+(p)/p$ is negative, which means that the corresponding waves propagate in the same direction as the current, from right to left, see (3.1). For positive p, we have $pU < 0$. Therefore, it is possible that $\Omega_S^+(p) = 0$ at a certain positive p for some values of the parameters of these waves. The equation $\Omega_S^+(p) = 0$ yields the following equation with respect to p:

$$\rho_1 pU^2 = EIp^4 + \rho_1 g. \tag{4.5}$$

This equation has no roots for $|U| < U_c$, two roots for $|U| > U_c$ and one double roots for $|U| = U_c$, where U_c is such that the derivatives in p of the left-hand and right-hand sides are equal

$$\rho_1 U^2 = 4EIp^3. \tag{4.6}$$

https://doi.org/10.1017/jfm.2025.10268 Published online by Cambridge University Press

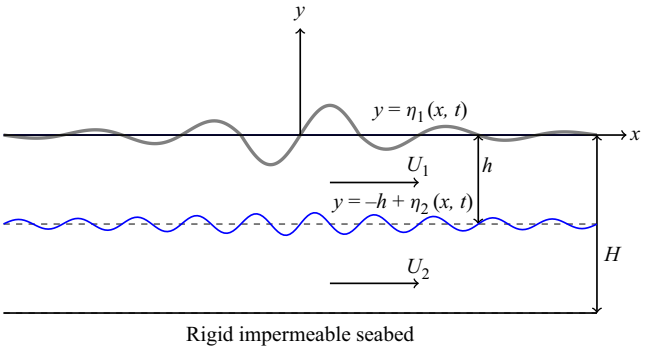


Figure 1. Schematic diagram of the physical domain representing a two-layer fluid with a plate-covered surface and interface.

Substituting (4.6) in (4.5), we find $p_c^4 = (\rho_1 g/3EI)$, and then (4.6) provides

$$U_c = -\left(\frac{4g}{3}\right)^{1/2}\left(\frac{3EI}{\rho_1 g}\right)^{1/8}. \tag{4.7}$$

The parameters of the problem, which will be used below, are $g = 9.81\ \mathrm{m\,s^{-2}}$, $E = 5 \times 10^8$ Pa, $\rho_1 = 1003.5\ \mathrm{kg\,m^{-3}}$, $\rho_2 = 1024\ \mathrm{kg\,m^{-3}}$, $\nu = 0.3$ and $d = 1$ cm providing $I = 45.78$ $\mathrm{m^3}$ and $U_c = -2.127\ \mathrm{m\,s^{-1}}$. Therefore, the waves of the system $\Omega_S^+(p)$ propagate in the direction of the current for negative p and in the opposite direction for positive p if $|U| < U_c$. For positive p and $|U| > U_c$, waves with $0 < p < p_1$ and $p > p_2$, where $p_2 > p_1 > 0$ are the roots of (4.5), propagate opposite to the current, and waves with $p_1 < p < p_2$, propagate in the same direction as the current.

Equation (4.4) gives $\Omega_S^+(-p) = -\Omega_S^-(p)$, which means that the wave system with $\Omega_S^-(p)$ does not require special analysis. The waves with $p = \pm p_1$ and $p = \pm p_2$ have zero phase speeds and zero frequencies for the wave systems $\Omega_S^+(p)$ and $\Omega_S^-(p)$, respectively, see figure 2. Note also that waves with Ω, p and $-\Omega$, $-p$ are the same wave, see (3.1), propagating in the same direction and having the same frequency and wavelength. The waves corresponding to $\Omega_S^+(p)$ with positive Ω are shown in figure 2 by the solid line, and their 'mirror' images corresponding to $\Omega_S^-(p)$ are shown by dashed lines. For a moving oscillatory load on a floating elastic plate with frequency Ω, a single wave propagates in both the following and opposing directions of the load velocity for $U < -1.4\ \mathrm{m\,s^{-1}}$ and $\Omega > 0$. When $U > -1.4\ \mathrm{m\,s^{-1}}$, within the blocking points, three waves are present: two with positive group velocity and one with negative group velocity, all propagating in the opposite direction to the load. Nevertheless, a single wave propagates in the direction of the load.

The group velocity of the flexural-gravity waves on the current with $U < 0$ is given by

$$c_g^{\pm}(p) = \frac{\mathrm{d}\Omega_S^{\pm}}{dp} = -|U| \pm \frac{1}{2\sqrt{\rho_1|p|}}\frac{5EIp^4 + \rho_1 g}{\sqrt{(EIp^4 + \rho_1 g)}}sgn(p), \tag{4.8}$$

where $sgn(p) = -1$ for $p < 0$ and $sgn(p) = +1$ for $p > 0$.

It is seen that $c_g^+(p) < 0$ for $p < 0$ and $c_g^+(p)$ may change its sign for $p > 0$. Correspondingly, $c_g^-(p) < 0$ for $p > 0$. Let us find the roots of the equation $c_g^+(p) = 0$. The roots are positive. It is convenient to introduce a new unknown α as $EIp^4 = \rho_1 g\alpha$.

https://doi.org/10.1017/jfm.2025.10268 Published online by Cambridge University Press

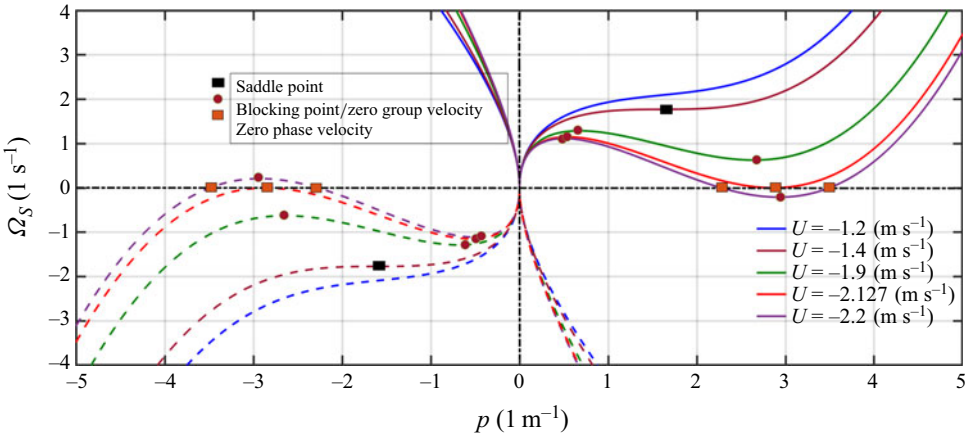


Figure 2. The dispersion curves Ω_S^+ (solid lines) and Ω_S^- (dashed lines) for different values of current velocity.

Then the equation $c_g^+(p) = 0$ reads

$$\frac{5\alpha + 1}{\alpha^{1/8}(\alpha + 1)^{1/2}} = \frac{4}{3^{3/8}} \frac{|U|}{|U_c|}. \tag{4.9}$$

The left-hand side of (4.9) is a smooth and positive function of α, which tends to $+\infty$ as $\alpha \to 0$ and as $\alpha \to \infty$. The left-hand side of (4.9) is minimum at $\alpha = \sqrt{1 + 1/15} - 1$, where it is equal to 1.7557. Therefore, (4.9) has no roots for $|U| < 0.6627|U_c|$. For larger speeds of the current, there are two roots of (4.9), which provide two wavenumbers of the waves with zero group speed and frequency. Note that both the phase and group velocities vanish for current speed U_c at a certain wavenumber, as given in (4.7). It is recalled that wave blocking occurs when the group velocity vanishes. We conclude that, for the selected parameters of the problem, there are no waves with zero phase speed if the speed of the current is smaller than 2.127 m s^{-1}, and there are no wave blocking for current speed smaller than 1.4 m s^{-1}. Abnormal waves occur only at relatively high speeds of the current. Note that the group velocity of the flexural-gravity wave remains continuous here, regardless of the current speed. This contrasts with the jump discontinuity observed at extreme values of plate compression, as discussed in Das *et al.* (2018*c*). For example, Lin (2021) reported that the speed of the under-ice current can be larger than 1.2 m s^{-1} flowing south-eastward from the coastal regions of southern Newfoundland towards deep waters.

In figure 2, the roots of (4.8) are shown by brown circles for $U = -1.9$ m s^{-1}. The primary blocking point is associated with the lower values of the wavenumber, whereas the other is known as the secondary blocking point, (see Boral *et al.* 2023*b*). Figure 2 reveals that, for any frequency within the primary and secondary blocking points, the dispersion relation (4.2) possesses three positive real wavenumbers, p, of the waves. By analysing the slopes of the three roots, it is confirmed that the first and the last waves are associated with positive group velocity, whilst the middle wave corresponds with negative group velocity. This implies that the middle wave propagates in the opposing direction to the current, whilst the wave energy, known as the group velocity, propagates in the direction of the current. The three roots of the dispersion relation merge at the saddle point, marked with a black square, for $U = -1.4$ m s^{-1}. Moreover, figure 2 demonstrates that wave blocking occurs for negative frequency Ω_S^+ and positive wavenumber p_3 lying in the range $p_1 < p_3 < p_2$ for $|U| > U_c$. This can be interpreted as waves in the range

https://doi.org/10.1017/jfm.2025.10268 Published online by Cambridge University Press

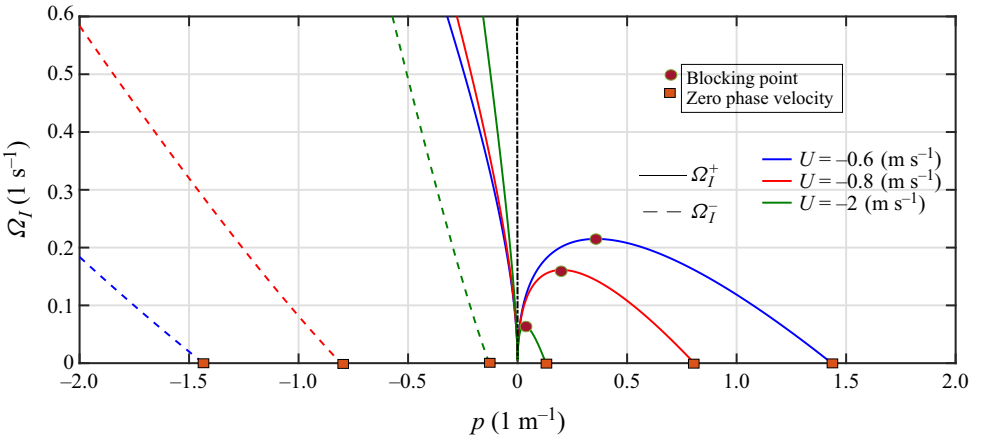


Figure 3. The dispersion curves for positive Ω_I^+ (solid lines) and Ω_I^- (dashed lines) with different values of current speed U.

$p_3 < p < p_2$ propagating in the direction of the current, whereas wave energy propagates in the opposite direction. On the contrary, both the wave energy and wave in the range $p_1 < p < p_3$ propagate in the direction of the current.

The dispersion relation (4.3), which is for waves localised at the interface between two infinitely deep fluids, gives two wave systems

$$\Omega_I^{\pm} = pU \pm \sqrt{rg|p|}. \tag{4.10}$$

For $U < 0$, the frequency $\Omega_I^+ > 0$ for $p < 0$ and the phase speed Ω_I^+/p is negative, which implies that the short interfacial wave propagates in the direction of current, see (3.1). For positive p, the expression $pU < 0$. Thus, the frequency Ω_I^+ may be zero for certain values of p, which is given by

$$p_c = rg/U^2. \tag{4.11}$$

Equation (4.11) provides that p_c approaches zero for large values of current speed U, see figure 3. Figure 3 is plotted by taking the same parameters used in figure 2. Equation (4.10) gives $\Omega_I^+ < 0$ for $p > p_c$, which implies that the phase speed is negative. Equation (4.10) provides $\Omega_I^+(p) = \Omega_I^-(-p)$, which means that $\Omega_I^- > 0$ for $p < -p_c$ in the case of $p < 0$, as presented by dashed lines in figure 3. Note that, in figure 3, only the positive values of $\Omega_I^+(p)$ and $\Omega_I^-(p)$ are exhibited. This is due to the fact that $\Omega_I^+(p) = \Omega_I^-(-p)$, which means that no additional analysis is needed for $\Omega_I < 0$.

The following group velocity for the short interfacial waves is obtained:

$$c_g^{\pm} = \frac{\mathrm{d}\Omega_I^{\pm}}{dp} = -|U| \pm \frac{1}{2}\sqrt{\frac{rg}{|p|}}sgn(p). \tag{4.12}$$

Equation (4.12) gives $c_g^- < 0$ for $p < 0$. It is obvious that the group velocity becomes zero, $c_g^+ = 0$, for positive wavenumber $p = p_{cg} = p_c/4$. Equation (4.11) implies that no wave blocking occurs for infinitely large values of current U, as demonstrated in figure 3. Furthermore, (4.12) gives that group velocity is positive for waves in the range $0 < p < p_{cg}$, and negative for $p_{cg} < p < p_c$. Equations (4.9) and (4.12) imply that flexural-gravity wave blocking occurs beyond a certain value of uniform current; however, wave blocking occurs in the short interfacial wave in the presence of a uniform current in a two-layer fluid. In figure 3, the wavenumbers p_c and p_{cg} are shown. Figure 3 demonstrates that interfacial

https://doi.org/10.1017/jfm.2025.10268 Published online by Cambridge University Press

waves do not propagate opposite to the current for frequencies beyond the blocking point. For any positive frequency, before the blocking point, two interfacial waves with positive and negative group velocities propagate in the opposite direction to the current. Moreover, two interfacial waves with negative group velocity propagate in the direction of the current for any frequency Ω_I.

4.2. *Moving upper layer over a stationary lower layer*

The dispersion relation (3.15) for a moving upper layer with speed U over a stationary lower layer provides, within the deep-water approximations,

$$(\rho_1\Omega_{r1}+\rho_2\Omega)\,\rho_1\Omega_{r1}^2\Omega+\{\rho_1\Delta U\Omega_{r1}-(\rho_2-\rho_1)g\}\,\rho_1 p\Omega_{r1}^2+\mathcal{A}\mathcal{D}_{r_1}=0, \tag{4.13}$$

where $\mathcal{A}=EIp^4+\rho_1 g$ and $\mathcal{D}_{r1}=-\rho_2\left\{sp\Omega\Omega_{r1}+p\Omega^2-(1-s)gp^2\right\}-\rho_1\Delta U p^2\Omega_{r1}$ with $\Omega_{r1}=\Omega-pU_1$. This limiting dispersion relation can be decomposed as

$$(\Omega_{r1}^2-\Omega_{r1+}^2)\left\{\rho_2\Omega_I^2+\rho_1\Omega_{r1}\Omega_I+\rho_1\Delta U|p|\Omega_{r1}-(\rho_2-\rho_1)g|p|\right\}=0, \tag{4.14}$$

where

$$\Omega_{r1+}^2=\frac{|p|}{\rho_1}(EIp^4+\rho_1 g), \tag{4.15}$$

$$\Omega_I^{\pm}=\frac{Ups\pm\sqrt{g|p|(1-s^2)-sp^2U^2}}{(1+s)}. \tag{4.16}$$

Equations (4.15) and (4.16) are associated with flexural-gravity waves where $\eta_{20}/\eta_{10}\ll 1$ and the interfacial wave with $\eta_{10}/\eta_{20}\ll 1$, respectively. It is worth mentioning that (4.15) is the same as in (4.4), which are both independent of the presence of the interface and the flow under the interface within the short wave approximations. Here, Ω_I^+ and Ω_I^- represent the upper and lower branches of the dispersion curve, respectively. It is recalled that the Kelvin–Helmholtz (KH) instability of short internal gravity waves for given values of the upper-layer speed U occurs at wavenumber p_{KH}

$$p_{KH}=\frac{g(1-s^2)}{sU^2}. \tag{4.17}$$

Equation (4.17) implies that p_{KH} approaches zero for large values of U for given values of s. Besides, p_{KH} approaches zero when the densities of the two layers are close to each other, $s\to 1$. The occurrences of KH instability are shown in figure 4 for different values of upper-layer speed. The parameters of the floating plate and liquid are considered the same as in figure 2. A detailed study on KH instability can be found in Cushman-Roisin (2005) for surface gravity waves and in Boral *et al.* (2021*b*) for capillary-gravity waves in a two-layer density-stratified fluid with tangential discontinuity of velocity across the mean free interface. The dispersion relation (4.16) for the interfacial waves with $|p|<p_{KH}$ reduces to

$$\Omega_I^{\pm}=\frac{Usp\pm U\sqrt{s|p|(p_{KH}-|p|)}}{1+s}. \tag{4.18}$$

Without loss of generality, the upper-layer velocity, which moves from right to left, is considered negative. Therefore, $pU>0$ for $p<0$, which implies that $\Omega_I^-(p)>0$. Consequently, the phase speed $c_I^-(p)=\Omega_I^-(p)/p$ is negative. It is checked that $\Omega_I^-(p)=0$ for $p_c=p_{KH}/(1+s)$, which are marked with orange squares in figure 4. For $U<0$. Equation (4.18) gives that $\Omega_I^-<0$ for $p_c<p<p_{KH}$. Note that $\Omega_I^+(p)=\Omega_I^-(-p)$, which implies that $\Omega_I^+>0$ for waves in the range $-p_{KH}<p<-p_c$ with p

https://doi.org/10.1017/jfm.2025.10268 Published online by Cambridge University Press

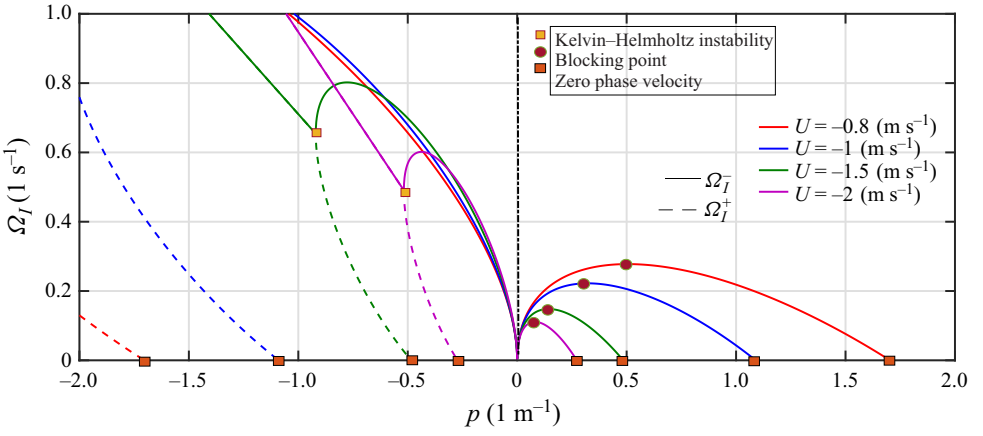


Figure 4. Short interfacial wave dispersion curve (4.16) in a two-layer fluid having a tangential discontinuity of velocity across the interface for different values of upper-layer speed U.

being negative. These waves are exhibited by dashed lines in figure 4. For interfacial waves within $0 < p < p_{KH}$, the group velocity is positive for $p < p^*$

$$p^* = \frac{p_{KH}}{2}\left(1 + \sqrt{\frac{s}{1+s}}\right), \tag{4.19}$$

and it is negative for $p^* < p_{KH}$. This implies that the interfacial wave propagates in the opposite direction to the current, whilst the corresponding wave energy propagates in the direction of the current. Similarly, for $-p_{KH} < p < 0$, it can be checked that the group velocity is negative for $p_* < -p$ and it is positive for $-p_{KH} < p_*$, where

$$p_* = -\frac{p_{KH}}{2}\left(1 + \sqrt{s/(1+s)}\right). \tag{4.20}$$

In figure 4, the waves with zero group speed are marked with brown circles, where wave blocking occurs. Figure 4 reveals that no interfacial wave propagates in the opposing direction to the upper-layer speed for frequencies beyond the blocking point. Additionally, two interfacial waves of positive and negative group velocity exist for any frequency before the occurrence of wave blocking for $p > 0$. However, two interfacial waves propagate in the direction of the upper-layer speed for frequencies prior to the occurrence of KH instability at $\Omega_I^- < \Omega_I^-(p_{KH})$. It is found that, for frequencies within the range $\Omega_I^-(p_{KH}) < \Omega_I^- < \Omega_I^-(p_*)$, two interfacial waves propagate in the direction of upper-layer speed. However, their group velocities are of opposite signs.

4.2.1. *Time-domain simulation*

Here, we simulate the flexural-gravity and internal gravity wave profiles when the upper layer is moving over a stationary lower layer in the time domain. Deep-water approximations are considered in both the upper and lower layers. The parameters are taken the same as in figure 4. Waves propagating in the direction opposite to the current are only considered for clarity. Equations (4.15) and (4.16) reveal that the flexural-gravity wave on the plate-covered surface and the interfacial wave on the interface are independent of each other under the assumption of deep-water approximation.

https://doi.org/10.1017/jfm.2025.10268 Published online by Cambridge University Press

Subsequently, using the Fourier integral, the plate deflection can be written (see Das *et al.* 2018*b*)

$$\eta_1(x,t) = \mathrm{Re}\left\{\int_0^\infty \hat{f}(p) e^{\mathrm{i}(px-\Omega_s t)}\,\mathrm{d}p\right\}, \tag{4.21}$$

where Ω_s is the frequency obtained from (4.15) for a given incident wave with wavenumber p. The function $\hat{f}(p)$ is the Gaussian wavepacket in the transform space, which is defined as

$$\hat{f}(p) = 2A\sqrt{\pi b}\, e^{-b(p-p_a)^2}, \tag{4.22}$$

where p_a is the centre wavenumber, $A = 0.3$ m is the amplitude and $b = 2000$ m^2 is the spreading function.

From (3.7), the amplitude ratio is obtained

$$a(p) \equiv \frac{\eta_{20}}{\eta_{10}} = \frac{2s\Omega_{r1}^2}{e^{ph}\left\{\Omega_I^2 + s\Omega_{r1}\Omega_I - g(1-s)p + spU\Omega_{r1}\right\}}. \tag{4.23}$$

Thus, the displacement of the interfacial wave is written as

$$\eta_2(x,t) = \mathrm{Re}\left\{\int_0^\infty a(p)\hat{f}(p) e^{\mathrm{i}(px-\Omega_I^+ t)}\,\mathrm{d}p\right\}. \tag{4.24}$$

We consider the upper-layer speed $U = -0.5$ m s^{-1} and two different values of centre wavenumber, $p_a = 0.1$ 1 m^{-1} (before the occurrence of wave blocking) and $p_a = 0.2$ 1 m^{-1} (after the occurrence of wave blocking), see figure 6(*a*).

In figures 5(*b*)–5(*f*), the time-domain simulation of the flexural-gravity waves in blue and interfacial waves in red are exhibited for $p_a = 0.1$ 1 m^{-1}. It is observed that the group velocity of the flexural-gravity wave is higher than that of the interfacial wave, and both waves are propagating to the right. Figures 6(*a*) and 6(*b*) are taken from 'Movie FGW', and figures 5(*c*)–5(*f*) are taken from 'Movie IGW figures 5, which are available at https://doi.org/10.1017/jfm.2025.10268. On the other hand, in figure 6, only the time-domain simulation of the interfacial wave for $p_a = 0.2$ 1 m^{-1} is shown. These figures are taken from 'Movie IGW figure 6', which is also available in the supplementary material. Figure 6 reveals that the interfacial wave packet moves to the left due to negative group velocity, whereas the phase velocity is positive. This is obvious from the dispersion curve, see figure 6(*a*), since the slope of the interfacial wave dispersion curve is negative beyond the blocking point.

5. Flexural-gravity wave and interfacial wave relation: wave blocking

The present section deals with analysing the occurrence of wave blocking for flexural-gravity waves interacting with the interfacial wave in the presence of current in finite water depth H. The dispersion relation of these waves in the presence of a tangential discontinuity of velocity across the interface is given by (3.8). Note that the flexural-gravity and interfacial waves are analysed individually under deep-water approximations in § 4, since they are uncoupled. It may be recalled that wave blocking occurs when the speed of wave energy propagation, which is known to be the group velocity, $d\Omega/dp$, vanishes (see Boral *et al.* 2023*b*). Thus, the existence of extrema in the dispersion curve of Ω as a function of wavenumber p implies the occurrence of wave blocking, as discussed in § 4. Mathematically, the roots of the dispersion relation coalesce at the blocking point. The study on wave blocking is crucial to understanding the behaviour of the roots of the

https://doi.org/10.1017/jfm.2025.10268 Published online by Cambridge University Press

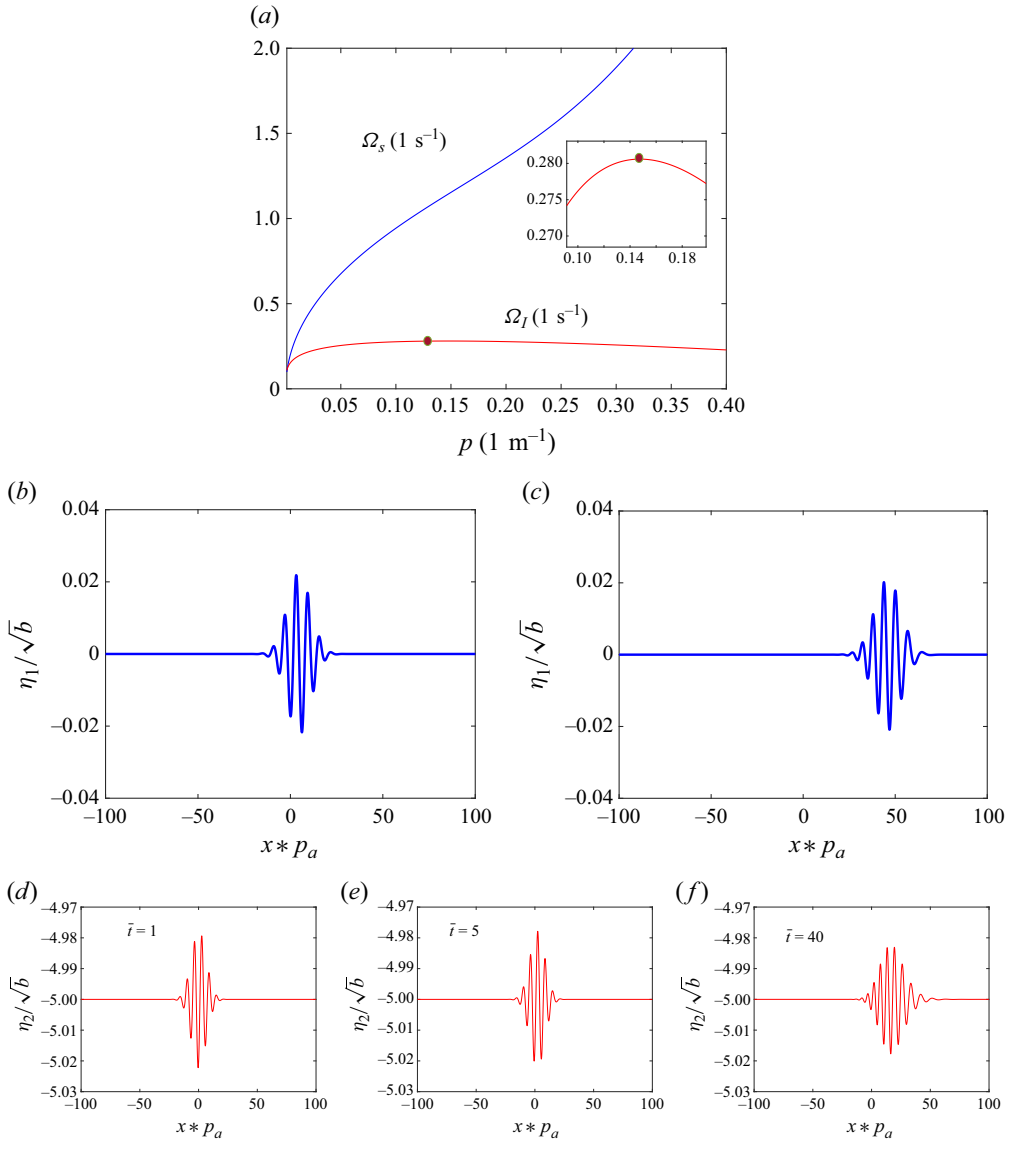


Figure 5. (*a*) Dispersion curve, and (*b–f*) time-domain simulation of the waves for two different times are shown. In (*b*) and (*c*), the flexural-gravity wave profiles are exhibited and in (*d*), (*e*) and (*f*) the interfacial wave profiles are shown for $p_a = 0.1\ 1\ \mathrm{m}^{-1}$. Note that here non-dimensional time is set as $\bar{t} = U p_a t$.

dispersion under the influence of varying ocean currents in upper and lower layers. This section is divided into subsections based on the speed of the upper layer with respect to the lower layer.

This section provides clearer insights into the occurrences of wave blocking in flexural-gravity and interfacial waves in the presence of uniform and varying currents in a two-layer fluid of finite depth. Other special cases, such as a finite upper layer in an infinite depth lower layer and shallow upper and lower layers, can be studied in a similar way by simplifying the dispersion relation (3.8). The parameters are selected as $g = 9.81\ \mathrm{m\,s}^{-12}$, $E = 5 \times 10^9$ Pa, $\rho_1 = 1003.5\ \mathrm{kg\,m}^{-3}$, $\rho_2 = 1024\ \mathrm{kg\,m}^{-3}$, $\nu = 0.3$, $d = 0.1$ m, $h = 5$ m and

https://doi.org/10.1017/jfm.2025.10268 Published online by Cambridge University Press

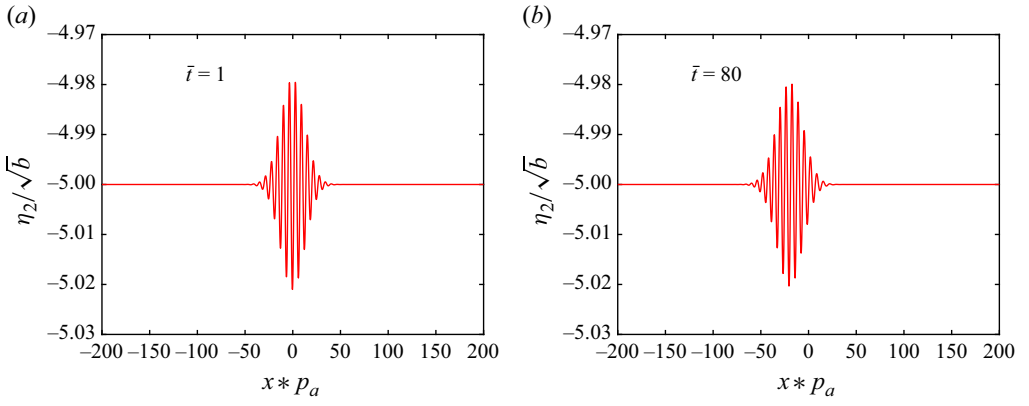


Figure 6. Time-domain simulation of the interfacial waves for two different times with $p_a = 0.2\ 1\ \mathrm{m}^{-1}$.

$H = 10$ m, providing $s = 0.9$ and $h/H = 0.5$, unless otherwise mentioned. Note that the choice of parameters is consistent with the work of Das *et al.* (2018*c*).

5.1. *Uniform current in the upper and lower layers*

Here, the speed of the upper layer is considered to be the same as that of the lower layer, which corresponds with a uniform current with velocity U beneath the thin floating elastic plate in a two-layer fluid. Note that the current velocity U is considered negative, which means that physical phenomena where the wave and current propagate in opposite directions are exhibited in the first quadrant of the $\Omega - p$ plane. One considers U as positive, providing a mirror image of the subsequent results about the line $p = 0$ without changing the physical meaning. The dispersion relation (3.10) is analysed by taking $\tau = 0$ to determine the criteria for the occurrences of wave blocking in flexural-gravity and interfacial waves in finite water depth. For clarity, the dispersion curves for positive frequencies are presented. Note that high current speeds, U, are considered in this section, although uncommon in real ocean conditions, which is crucial for theoretical analysis. This helps explore the wave dynamics under extreme scenarios, providing insights into interactions between wave modes, current shear and the interface's response. This theoretical framework can be applied to practical situations, such as studying the response of a floating plate to a moving load with appropriate modification in the mathematical formulation. High-speed currents simulate rapid moving forces on floating structures, allowing a better understanding of energy transfer, shear-induced instabilities and wave interactions, with relevance to dynamic loading in engineering and oceanography.

Figure 7 demonstrates the dispersion curves (3.10), (4.2) and (4.3) for a flexural-gravity wave with $U = -5\ \mathrm{m\,s}^{-1}$ and interfacial wave with $U = -0.7\ \mathrm{m\,s}^{-1}$. These figures depict the changes in the wave characteristics with changes in the depths of the upper and lower layers. Figure 7(*a*) reveals that the variations in the flexural-gravity wave characteristics in the direction of the current are minimal in deep water at finite depth. However, a strong interaction between the opposing current and flexural-gravity wave is observed in deep water at finite water depth for wavenumbers within the range $0 < ph < 1.5$, leading to conditions where the wave energy is redistributed or dissipated. It is found that wave blocking occurs in short flexural-gravity waves with opposing currents for certain values of frequency and wavenumber, representing a physical phenomenon where the wave energy cannot overcome the opposing flow. However, no wave blocking occurs in the flexural-gravity wave at finite water depth. Thus, the occurrence of wave blocking and interaction

https://doi.org/10.1017/jfm.2025.10268 Published online by Cambridge University Press

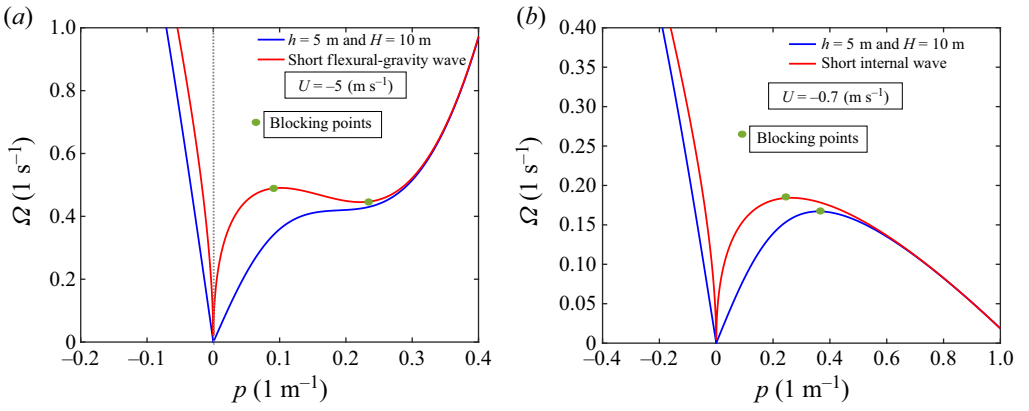


Figure 7. Dispersion curves (3.10), (4.2) and (4.3) for (*a*) flexural-gravity waves with $U = -5\ \mathrm{m\,s^{-1}}$ and (*b*) interfacial waves with $U = -0.7\ \mathrm{m\,s^{-1}}$.

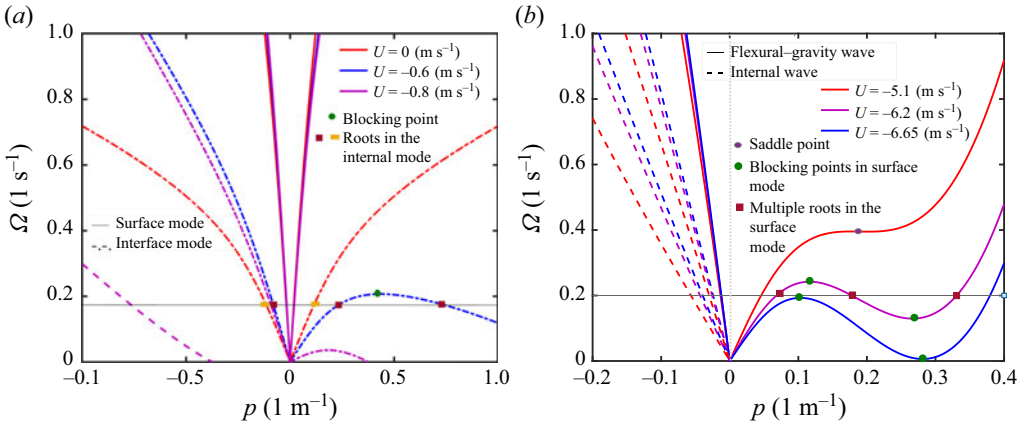


Figure 8. Dispersion curve (3.10) for waves on the plate-covered surface and interface in finite water depth for (*a*) $U = 0,\ -0.6$ and $-0.8\ \mathrm{m\,s^{-1}}$, and (*b*) $U = -5.1,\ -6.2$ and $U = -6.65\ \mathrm{m\,s^{-1}}$.

of multiple waves on the plate-covered surface depends on the depths of the upper and lower layers for given values of uniform current. On the other hand, figure 7(*b*) exhibits a minimal variation for the interfacial waves in deep water at finite water depth in the direction of current. This suggests that the stratified layers allow smooth propagation of the interfacial waves in the direction of the current, with negligible resistance or energy redistribution. Conversely, a pronounced variation in the interfacial wave with an opposing current is observed with changes in upper- and lower-layer depths for wavenumbers within the range $0 < ph < 3$. Figure 7(*b*) reveals that wave blocking occurs for lower values of frequency and higher values of wavenumber in the interfacial wave with opposing current in the case of finite water depth compared with deep water. This implies that the frequency beyond which interfacial waves do not propagate in the opposite direction to the current reduces as the depth of the upper and lower layers is reduced.

Figure 8 depicts the frequency Ω as a function of wavenumber p given by (3.10) for different values of current speed U. In figures 8(*a*) and 8(b), solid and dashed lines represent the flexural-gravity waves and interfacial waves, respectively. Figure 8(*a*) reveals that the dispersion curves associated with the flexural-gravity and interfacial waves are

https://doi.org/10.1017/jfm.2025.10268 Published online by Cambridge University Press

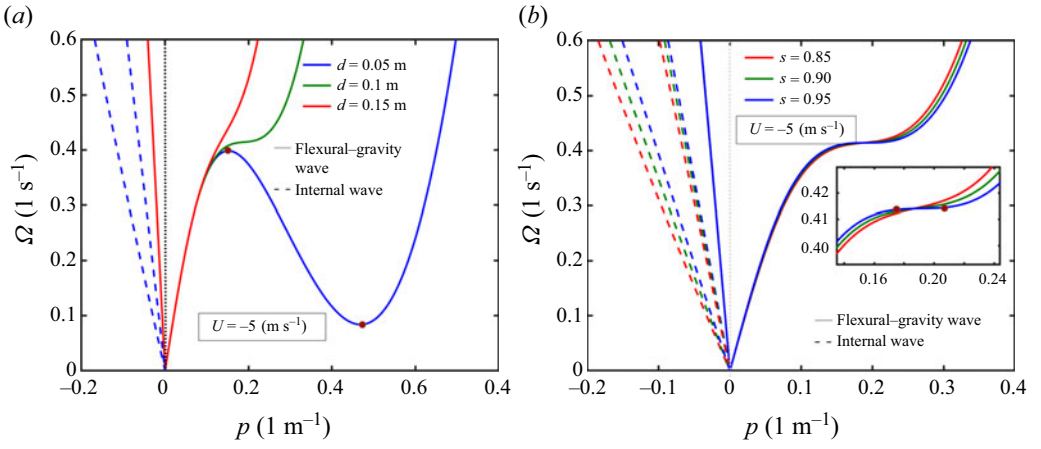


Figure 9. Dispersion curves (3.10) for waves on the plate-covered surface and interface in finite water depth for (*a*) different values of plate thickness d and (*b*) density ratio s for $U = -5\ \mathrm{m\,s^{-1}}$.

symmetric about the vertical line $p = 0$ in the absence of current. This symmetry reflects that waves behave identically in both directions. However, the dispersion curves become asymmetric in the presence of uniform current velocity $U\,(< 0)$. Figure 8(*a*) demonstrates that variations in the flexural-gravity waves are minimal in both the downstream (with the current) and upstream (against the current) directions, indicating that the current has a negligible effect on their propagation characteristics. Additionally, no wave blocking occurs in the flexural-gravity waves since no extrema exists in the dispersion curve. In contrast, wave blocking occurs in the interfacial wave where the dispersion curve possesses a maximum, which shifts to lower values of frequency and wavenumber p for higher values of current speed U. This indicates that stronger opposing currents reduce the range of frequencies and wavelengths for which interfacial waves can propagate upstream. On the other hand, a comparison of figures 8(*b*) and 2 reveals that the saddle point occurs for higher values of uniform current, $U = -5.1\ \mathrm{m\,s^{-1}}$, with lower values of frequency, $\Omega = 0.3953\ 1\,\mathrm{s^{-1}}$, compared with deep upper and lower layers. In addition, the critical current speed U_c where the phase velocity attains zero minimum is reduced from -6.73 to $-6.67\ \mathrm{m\,s^{-1}}$ in finite water depth $H = 10$ m compared with deep water. For $U = -6.2\ \mathrm{m\,s^{-1}}$, primary and secondary wave blocking occurs, and multiple real roots exist within a range of frequencies, indicating complex wave interactions. These findings are consistent with the results shown in figure 2. Figure 8(*b*) exhibits that interfacial waves cannot propagate in the upstream but are instead carried downstream. This is not the case observed in short interfacial waves, since p_c in (4.11) approaches zero for infinitely large values of U, as shown in figure 3. Two interfacial waves propagate only in the direction of the current, irrespective of the values of frequency Ω. Notably, figures 8(*a*) and 8(*b*) illustrate that wave blocking does not occur simultaneously in the plate-covered surface and interface for given values of uniform current U and frequency Ω. This suggests that, when multiple waves are present, they may propagate either at the interface or on the plate-covered surface in the upstream direction, depending on the current speed and frequency.

In figure 9, the dispersion curves (3.10) for waves on the plate-covered surface and interface are presented for different values of plate thickness d and density ratio s in the presence of uniform current $U = -5\ \mathrm{m\,s^{-1}}$. Figure 9(*a*) demonstrates that the primary and secondary blocking points occur in the flexural-gravity wave with opposing current

https://doi.org/10.1017/jfm.2025.10268 Published online by Cambridge University Press

for $d = 0.05$ m. Note that a plate thickness of $d = 0.05$ m was used to represent grease ice in the laboratory experiment described by Carr *et al.* (2019). However, no wave blocking occurs in the flexural-gravity waves propagate in the upstream direction for $d = 0.1$ and $d = 0.15$ m. This means that a thinner plate makes it easier for the opposing current to interact with the waves, leading to situations where the energy of the waves is trapped, causing wave blocking within certain frequency ranges. Besides, negligible variations are observed in the flexural-gravity wave and interfacial wave dispersion curve when it propagates in the direction of current U. Similar to figure 8(b), in figure 9(a), interfacial waves do not propagate opposite to the current for each value of frequency Ω and plate thickness d with $U = -5$ m s^{-1}. This means that, at higher opposing current speeds, interfacial waves cannot move upstream because the current pushes the wave energy strongly downstream. On the other hand, figure 9(b) illustrates that wave blocking occurs in the flexural-gravity wave with opposing current $U = -5$ m s^{-1} for two closely situated frequencies Ω for density ratio $s = 0.95$ and $d = 0.1$ m. This implies that flexural-gravity wave blocking occurs for certain values of plate thickness, d, with a change in the values of density ratio s. The variations in the flexural-gravity and interfacial wave dispersion curves in the direction of current are similar to those of figure 9(a) with changes in the values of s. Figures 9(a) and 9(b) reveal that the interfacial wave with opposing current is not influenced by a change in the values of plate thickness d and density ratio s in the presence of higher values of uniform current U.

5.2. *Different current speed in the upper and lower layers*

This section delves into the analysis of wave blocking that occurs in the flexural-gravity wave and interfacial wave in a two-layer density-stratified fluid with different current speeds between the upper and lower layers. The upper layer is moving at a speed U_1, and the lower layer moves at a speed U_2 such that $U_1 \neq U_2$. Note that the case for $U_1 = U_2$ is studied in sub § 5.1. The speed of the lower layer is considered to be lower than that of the upper layer since the lower layer is heavy. The associated dispersion relation (3.8) for $\tau = 0$ is analysed. Emphasis is given to analysing the dispersion curves when the upper and lower layers are moving in opposite directions. This section provides deep insights into the occurrences of wave blocking in flexural-gravity waves and interfacial waves. Furthermore, the section provides the range of frequencies for which multiple wave interactions take place either on the plate-covered surface or on the interface, depending on the parameters. The occurrences of KH instability due to tangential discontinuity of velocity across the interface and its influence on the plate-covered surface are analysed. Figure 10 demonstrates frequency Ω as a function of wavenumber p given by dispersion relation (3.8) for different values of upper-layer speed U_1 over a stationary lower layer with $U_2 = 0$. Figure 10 reveals negligible variations among the flexural-gravity waves in the upstream and downstream directions of upper-layer velocities U_1. Wave blocking occurs in the interfacial waves propagating in the opposite direction of U_1 for certain values of wavenumber p, beyond which no interfacial waves propagates. Besides, KH instability occurs for certain values of wavenumber p in the interfacial wave, depending on the values of U_1, when waves propagate in the direction of upper-layer velocity. This instability arises from the mean flow discontinuity at the interface, where the shear between the layers creates a mechanism for energy exchange that destabilises the system. Before this instability occurs, wave blocking is observed, which highlights the complex interplay between the wave dynamics and shear-induced instabilities. A comparison of figures 10 and 4 depicts that the values of the wavenumber at which various physical phenomena like wave blocking, KH instability and zero phase speed occur shift to slightly lower values

https://doi.org/10.1017/jfm.2025.10268 Published online by Cambridge University Press

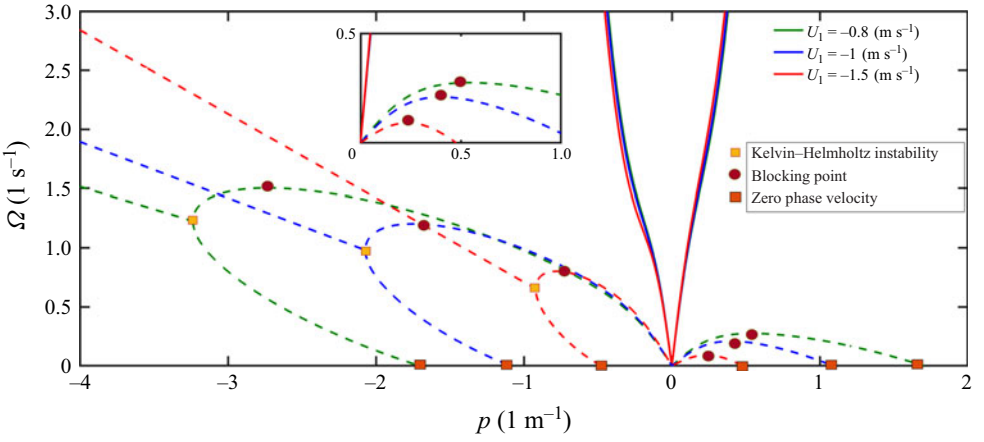


Figure 10. Dispersion curves (3.15) for waves on the plate-covered surface (solid lines) and interface (dashed lines) for different values of upper-layer speed U over a stationary lower layer.

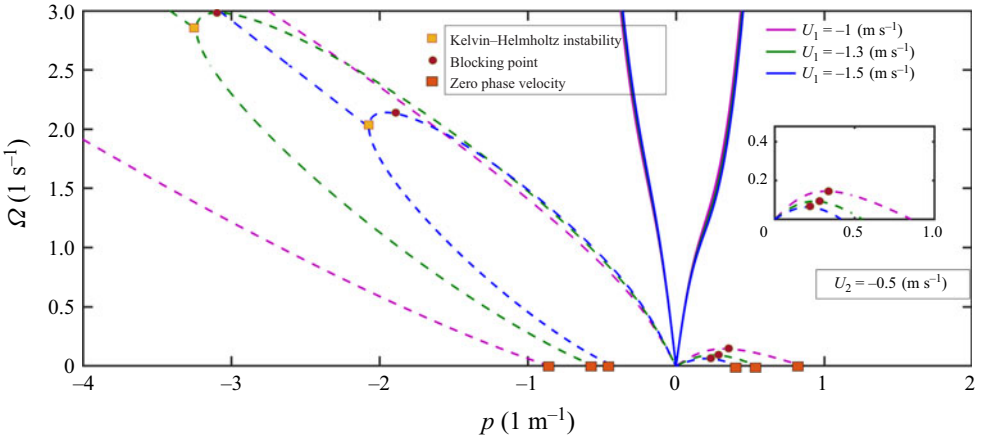


Figure 11. Dispersion curves (3.8) for waves on the plate-covered surface (solid lines) and interface (dashed lines) for different values of upper-layer speed U_1 with $U_2 = -0.5$ m s^{-1}.

in finite water depth. This implies that the interaction of the flexural-gravity wave with the interfacial wave reduces the interfacial wave speed in the following and opposing directions of upper-layer speed. Unlike the scenario shown in figure 8, where no blocking occurs for interfacial waves with the following uniform current, figure 10 demonstrates that wave blocking occurs even for short interfacial waves with higher frequencies when propagating in the direction of the upper-layer velocity. Physically, this implies that the interface acts as a barrier that modifies the energy propagation pathways and leads to instability in a two-layer fluid with a stationary lower layer.

In figure 11, a similar result as in figure 10 is plotted for $U_2 = -0.5$ m s^{-1}. Here, the reference case of moving upper and lower layers in the same direction from right to left is discussed. Figure 11 depicts an analogous observation with figure 10 for flexural-gravity wave propagation in the following and opposing directions of the upper-layer velocity. A comparison of figures 11 and 10 reveals that the values of positive wavenumber p, at which wave blocking and zero phase speed occurs in the interfacial wave for $U_1 = -1$ and -1.5 m s^{-1}, are significantly lower in the presence of lower-layer speed

https://doi.org/10.1017/jfm.2025.10268 Published online by Cambridge University Press

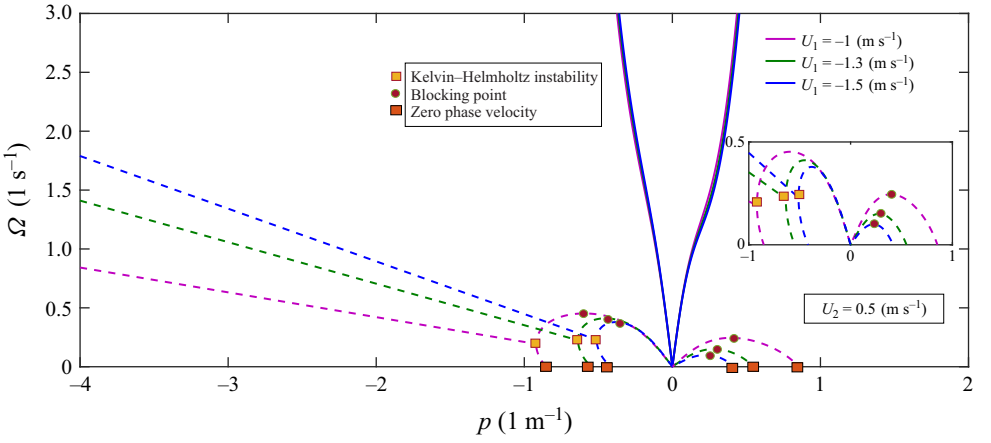


Figure 12. Dispersion curves (3.8) for waves on the plate-covered surface (solid lines) and interface (dashed lines) for different values of upper-layer speed U_1 with $U_2 = 0.5$ m s^{-1}.

$U_2 = -0.5$ m s^{-1}. Physically, this indicates that the additional motion of the lower layer reduces the relative velocity difference experienced by interfacial waves propagating in the direction opposite to the upper-layer flow. As a result, the wavelength and phase speed of these interfacial waves decrease, reflecting the enhanced influence of the moving lower layer in modulating the wave dynamics. On the other hand, KH instability and wave blocking occur for lower values of negative wavenumber p in the case of $U_2 = -0.5$ m s^{-1} than that of $U_2 = 0$ for $U_1 = -1$ and -1.5 m s^{-1}. This suggests that when the upper and lower layers flow at different speeds in the same direction, the velocity gradient at the interface becomes more pronounced, leading to increased shear effects. These effects allow shorter interfacial waves, which are associated with higher frequencies, to propagate with the flow.

In figure 12, similar results as in figure 11 are plotted by changing the direction of the lower-layer velocity with $U_2 = 0.5$ m s^{-1}. It is observed that the flexural-gravity wave in the following and opposing directions of the upper-layer speed is not affected by the change in direction of the lower-layer speed. A comparison of figures 12 and 11 shows that wave blocking and KH instability occur at lower frequencies and wavenumbers associated with the interfacial wave propagating in the direction of upper-layer speed. This is due to the increased shear at the interface, which amplifies instability and disrupts energy transfer, leading to earlier blocking of shorter, high-frequency interfacial waves. On the other hand, figure 12 illustrates that wave blocking occurs for slightly higher values of frequencies and wavenumbers when the interfacial waves propagate in the opposite direction to the upper-layer speed and in the same direction as the lower-layer speed compared with that of figure 11. Additionally, the wavenumbers at which phase speeds become zero in the interfacial waves shift slightly to higher wavenumber values in figure 12 for $U_2 = 0.5$ m s^{-1} compared with figure 11 with $U_2 = -0.5$ m s^{-1}. Figures 11 and 12 show that, when interfacial waves attempt to travel upstream (against the upper-layer speed), against the flow of the lower layer, they encounter significant resistance due to the opposing motion. However, when interfacial waves move downstream in the same direction as the lower layer's flow, the supporting motion of the current reduces the relative shear, allowing these waves, especially those with higher frequencies and shorter wavelengths, to propagate more effectively.

In figure 13, the frequency Ω as a function of wavenumber p given by (3.8) is studied for different values of lower-layer speed U_2 with the upper-layer speed $U_1 = -6$ m s^{-1}. The

https://doi.org/10.1017/jfm.2025.10268 Published online by Cambridge University Press

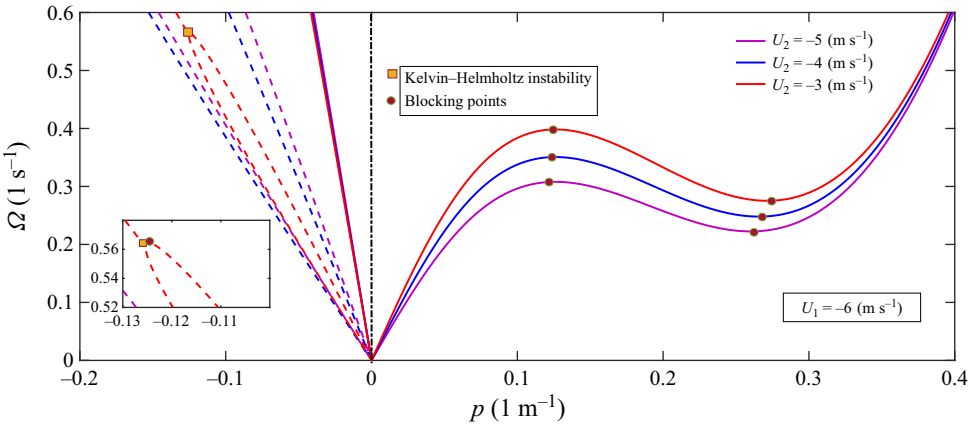


Figure 13. Dispersion curves (3.8) for waves on the plate-covered surface (solid lines) and interface (dashed lines) for different values of lower-layer speed U_2 with $U_1 = -6$ m s^{-1}.

lower layer is assumed to be moving in the direction of the upper-layer speed. Here, the current speeds are considered larger than those typically observed in the ocean, and this theoretical framework is crucial for understanding extreme interactions that may inform practical scenarios, such as the response of a floating plate to high-speed moving loads in a two-layer fluid. Physically, this figure shows that wave blocking for flexural-gravity waves with opposing upper-layer speed occurs at lower frequencies and wavenumbers when the shear across the interface is weaker. This suggests that a weaker velocity gradient at the interface reduces the energy required for blocking, making it easier for these waves to lose momentum. On the other hand, as the shear current strengthens, the primary and secondary blocking points shift to higher frequencies. Furthermore, the negligible variations in the flexural-gravity waves propagating in the direction of the upper-layer speed, irrespective of the shear strength, highlight that downstream propagation is less sensitive to current speed differences across the interface. Additionally, the interfacial waves cannot travel in the opposite direction to the upper-layer speed U_1 when the current speed is high, regardless of the speed of the lower layer U_2. This shows that the upper-layer current has a stronger influence on the wave movement at the interface.

Figure 14 demonstrates the variations in the dispersion curves associated with the interfacial waves for different values of the density ratio s. Here, the upper layer flows from right to left with $U_1 = -1.5$ m s^{-1}, while the lower layer is considered to move either in the same direction as the upper layer with $U_2 = -0.5$ m s^{-1} (dashed lines) or in the opposite direction with $U_2 = 0.5$ m s^{-1} (solid lines). The variations in the flexural-gravity waves with changes in density ratio s are negligible and are not presented here for clarity. Figure 14 reveals a qualitatively similar observation to that of figures 11 and 12. Figure 14 depicts that KH instability and wave blocking occur in the interfacial waves for smaller values of frequency Ω and wavenumber p with an increase in the values of density ratio s, regardless of the direction of the lower-layer velocity with respect to the upper-layer velocity. This can be interpreted as the higher values of the density ratio, s, implying weaker stratification, reducing the wavelength and phase speed of the interfacial wave for given values of frequency and wavenumber in a two-layer fluid with tangential discontinuity of velocity. Moreover, for higher values of s, particularly at $s = 0.95$, no interfacial wave propagation is observed in the direction opposite to the upper-layer flow, irrespective of the direction of the lower layer. This can be explained by the diminished stratification at high s, which suppresses the ability of the interfacial wave

https://doi.org/10.1017/jfm.2025.10268 Published online by Cambridge University Press

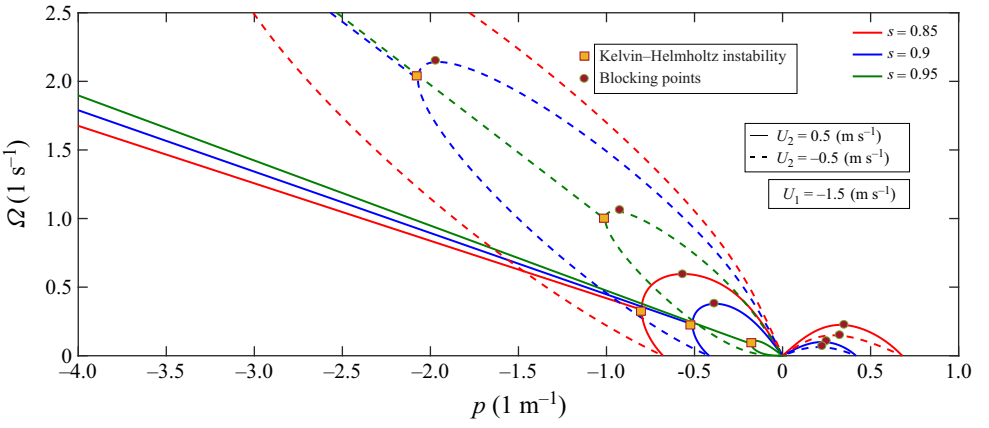


Figure 14. Dispersion curves (3.8) for waves on the interface with upper and lower layers moving in the same direction (dashed lines) and in the opposite direction (solid lines) for different values of density ratios s with $U_1 = -1.5$ m s^{-1} and $|U_2| = 0.5$ m s^{-1}.

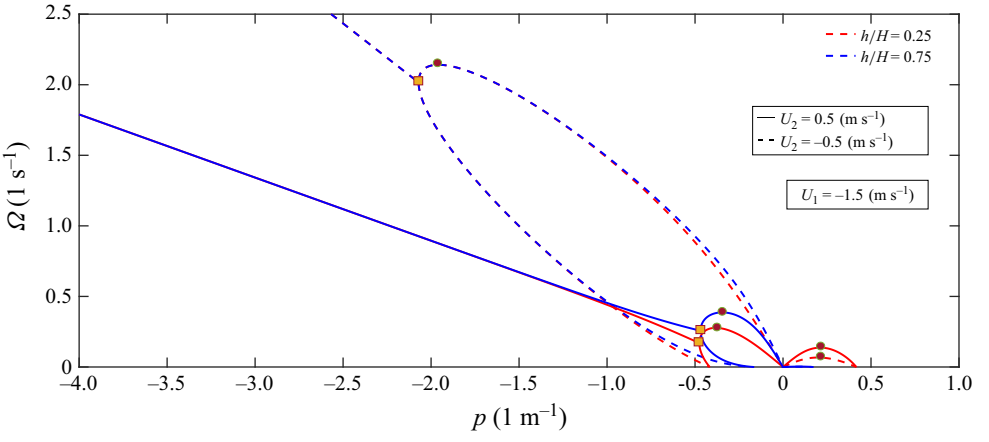


Figure 15. Dispersion curves (3.8) for waves on the interface with upper and lower layers moving in the same direction (dashed lines) and in the opposite direction (solid lines) for different values of water depth ratios h/H with $U_1 = -1.5$ m s^{-1} and $|U_2| = 0.5$ m s^{-1}.

to propagate against the current. It is noteworthy that the wavenumbers at which the phase speed vanishes depend on the density ratio s but are independent of the direction of the lower-layer velocity relative to the upper-layer velocity.

Similar to figure 14, in figure 15, the role of water depth ratio h/H in the variations of the interfacial wave dispersion curve is demonstrated. Figure 15 reveals that negligible variations are observed in the interfacial wave propagation in the direction of the moving upper and lower layers for $h/H = 0.25$ and $h/H = 0.75$. However, when the interfacial wave propagates in the same direction as the upper layer and opposite to the lower layer, KH instability and wave blocking occur at lower frequencies. For $h/H = 0.25$, the figure shows that interfacial waves do not propagate in the opposing direction of the upper-layer velocity. This indicates that, when the interface is close to the plate-covered surface, the shallow water depth (small h/H) limits the interfacial wave's ability to move opposite to the upper layer's current. On the other hand, for $h/H = 0.75$, the interfacial wave propagates in the opposite direction to the upper-layer flow within a

https://doi.org/10.1017/jfm.2025.10268 Published online by Cambridge University Press

certain range of frequency and wavenumber, regardless of the direction of the lower-layer flow. This is due to the increased water depth, which provides more space for the wave to propagate, reducing the influence of the plate-covered surface and allowing interfacial waves to propagate upstream. Figure 15 suggests that the wavelength and phase speed of the interfacial wave propagating with the upper-layer flow are highly influenced by the direction of the lower-layer flow in a two-layer fluid with tangential discontinuity of velocity across the interface.

6. Analysis of the dispersion relation in the presence of retardation time

In this section, the dispersion relations (3.10) and (3.15) are studied for a given non-zero value of retardation time τ. In general, each dispersion relation (3.10) and (3.15) possesses four real roots, four complex roots and infinitely many purely imaginary roots for $\tau = 0$, which is studied in § 5. However, when $\tau > 0$, which accounts for material retardation effects, the system loses its real roots, meaning propagating waves do not exist, for a given real frequency Ω. This is referred to as spatially damped waves, see Gerasik & Stastna (2010) and Mikaelyan (2017). Below, for $\tau > 0$, we consider temporally damped waves in which a real wavenumber p is mapped to a complex frequency $\Omega = \Omega_R + \mathrm{i}\Omega_I$. Note that, (3.8) implies that the group velocity, which is defined for non-dissipative media as $d\Omega(p)/\mathrm{d}p$, is complex in the presence of plate viscosity τ, and is referred to as complex group velocity, see Gerasik & Stastna (2010). The complex group velocity lacks a clear physical meaning and is often seen as a purely mathematical concept. Gerasik & Stastna (2010) stated that the complex group velocities associated with the temporally damped Klein–Gordon equation and electromagnetic waves in a partially conducting medium are related to the energy transport velocity. Furthermore, their study mentioned that the real part of group velocity, $\mathrm{Re}\{\mathrm{d}\Omega/\mathrm{d}p\}$, indicates the speed and direction of energy transport. While the imaginary part of group velocity, $\mathrm{Im}\{d\Omega/\mathrm{d}p\}$ evinces the spatial decay of the wave packet.

In figure 16, the variations of real and imaginary components of frequencies, as in the dispersion relation (3.10), for a temporarily damped flexural-gravity wave and interfacial wave, are exhibited. The results are shown for varying plate-viscosity parameters τ, under the influence of a uniform opposing current $U = -1\ \mathrm{m\,s^{-1}}$. As seen in figure 16($a$), the real part of the frequency Ω_{FGW} exhibits a non-monotonic behaviour in the presence of viscosity: it initially increases with wavenumber p, reaches a peak and then declines. This demonstrates that the real component of complex group velocity associated with flexural-gravity waves, $\mathrm{Re}\{\mathrm{d}\Omega_{FGW}/\mathrm{d}p\}$, changes sign from positive to negative as the values of wavenumber, p, increase and vanishes for a certain value of wavenumber. In contrast, for the case $\tau = 0$, Ω_{FGW} increases monotonically with p. Increasing the viscosity parameter τ leads to a reduction in the peak value of Ω_{FGW} and shifts the corresponding wavenumber to lower values, indicating a damping-induced modification of the wave propagation characteristics. This demonstrates that the real component of the complex group velocity associated with flexural-gravity waves, $\mathrm{Re}\{\mathrm{d}\Omega_{FGW}/\mathrm{d}p\}$, changes sign from positive to negative as the value of the wavenumber, p, increases and vanishes for a certain value of wavenumber. A qualitatively opposite trend to that of $\mathrm{Re}\{\Omega_{FGW}\}$ is observed in the imaginary component of frequency, $\mathrm{Im}\{\Omega_{IGW}\}$. On the other hand, figure 16(b) depicts that the real component of frequency associated with the interfacial wave, $\mathrm{Re}\{\Omega_{IGW}\}$, remains unaltered with change in the value of τ indicating that the wave energy transport speed is not sensitive to viscous effects in this regime. However, a negligible variation is observed in $\mathrm{Im}\{\Omega_{IGW}\}$ for lower values of wavenumber p in the presence of τ, signifying negligible damping of the interfacial waves. However, this

https://doi.org/10.1017/jfm.2025.10268 Published online by Cambridge University Press

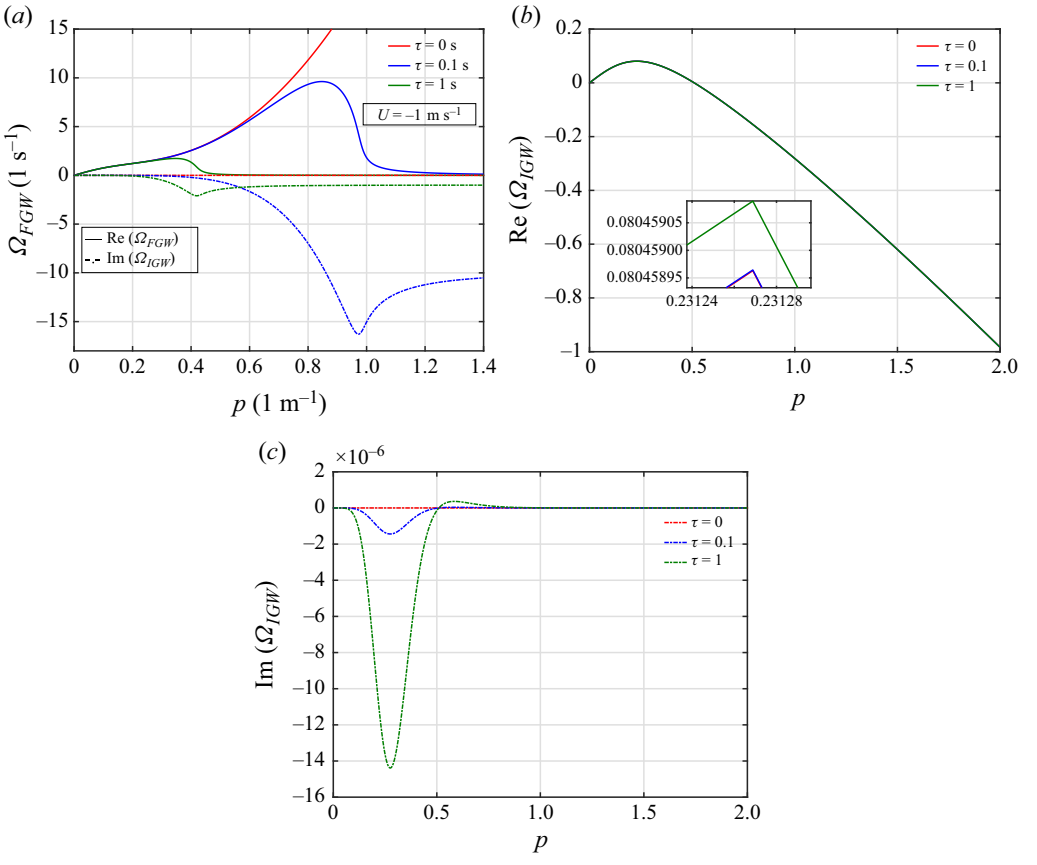


Figure 16. Variations of real and imaginary frequency components associated with the flexural-gravity wave (FGW) and interfacial wave (IGW) versus real wavenumber p for different values of plate viscosity τ with uniform current $U = -1\ \mathrm{m\,s^{-1}}$.

effect remains weak compared with the flexural-gravity wave, since the interface is located far away from the plate-covered surface. Figure 17 illustrates the dispersion relations for flexural-gravity waves in a two-layer fluid with a discontinuous background mean flow, comparing cases where the lower layer flows in the same direction as the upper layer, as shown in figure 17(*a*) and in the opposite direction to that shown in figure 17(*b*), where the upper layer moves with velocity $U_1 = -1.5\ \mathrm{m\,s^{-1}}$. Despite this variation in lower-layer velocity, the real and imaginary components of the frequency, Ω_{FGW}, exhibit nearly identical behaviours in both cases, and the results are qualitatively similar to that of figure 16(*a*). The negligible differences between figures 17(*a*) and 17(*b*) suggest that the wave dynamics in this configuration is predominantly governed by the motion of the upper layer and the plate viscosity, with only a weak sensitivity to the lower-layer flow.

For $\tau > 0$ with a given load frequency Ω, our study focuses on the loci of the roots (wavenumbers) of the dispersion relation in the complex plane. Among these roots, the 'predominant waves' are those with complex roots located close to the real axis, see Boral *et al.* (2021*a*). Physically, these waves have a significant phase velocity, indicated by the real part of their wavenumber, and moderate attenuation, represented by their imaginary part. These predominant waves are of practical interest since they dominate the observable wave motion. In contrast, 'rapidly decaying waves' have wavenumbers far from the real axis, causing them to dissipate quickly. In this section, the imaginary parts

https://doi.org/10.1017/jfm.2025.10268 Published online by Cambridge University Press

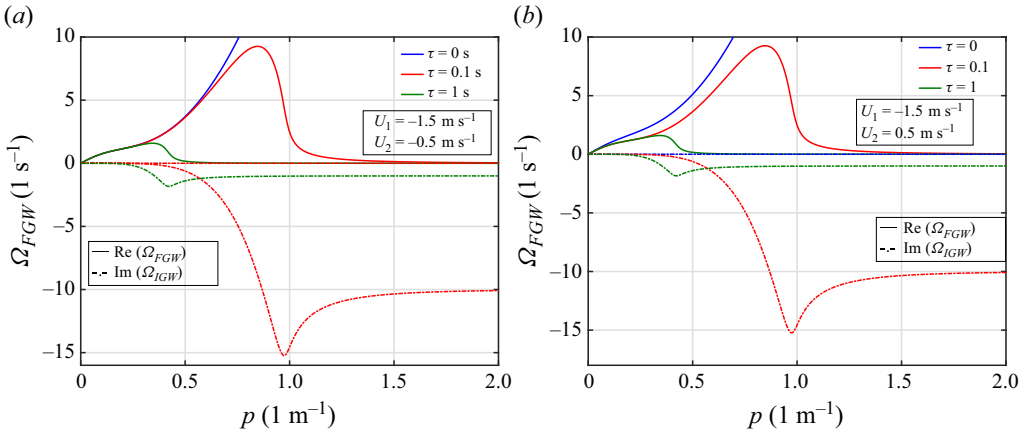


Figure 17. Variations of real and imaginary frequency components associated with the flexural-gravity wave (FGW) versus real wavenumber p for different values of plate viscosity τ with different speed of background mean flow, $U_1 = -1.5$ m s^{-1} and $|U_2| = 0.5$ m s^{-1}.

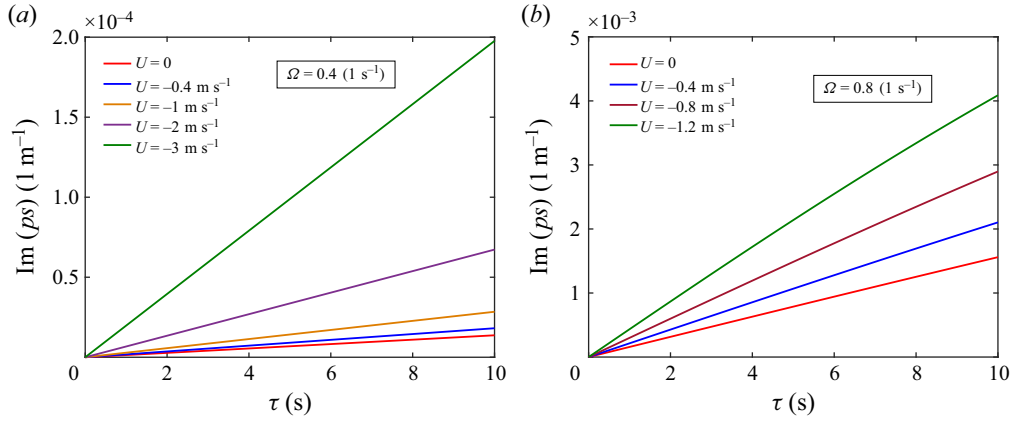


Figure 18. Variations of the imaginary part of the wavenumber, Im (p_S), associated with the plate-covered surface as in (3.10) as a function of τ for different values of current speed U with (a) $\Omega = 0.4$ 1 s^{-1} and (b) $\Omega = 0.8$ 1 s^{-1}.

of the wavenumbers associated with flexural-gravity waves, denoted by Im (p_S), with opposing uniform and varying currents, are analysed. Additionally, the loci of the roots of the interfacial wave are investigated for both the cases of uniform and varying currents for frequencies close to the blocking points, which cases are studied in § 5. The values of different parameters are considered to be the same as in § 5 for numerical computations unless further specified.

Figure 18 illustrates the variations in the imaginary part, Im (p_S), of the predominant root of the dispersion relation (3.10) associated with the flexural-gravity waves as a function of retardation time τ for different values of opposing uniform current speed U with $\Omega = 0.4$ 1 s^{-1} and $\Omega = 0.8$ 1 s^{-1}. It is observed that Im (p_S) remains zero for $\tau = 0$, regardless of the values of U and Ω, which is due to the existence of real roots of the dispersion relation (3.10) and is discussed in § 5. However, the values of Im (p_S) increase monotonically with an increase in the values of τ for all values of U, indicating that the wave attenuation becomes more pronounced with increasing retardation time. Moreover,

https://doi.org/10.1017/jfm.2025.10268 Published online by Cambridge University Press

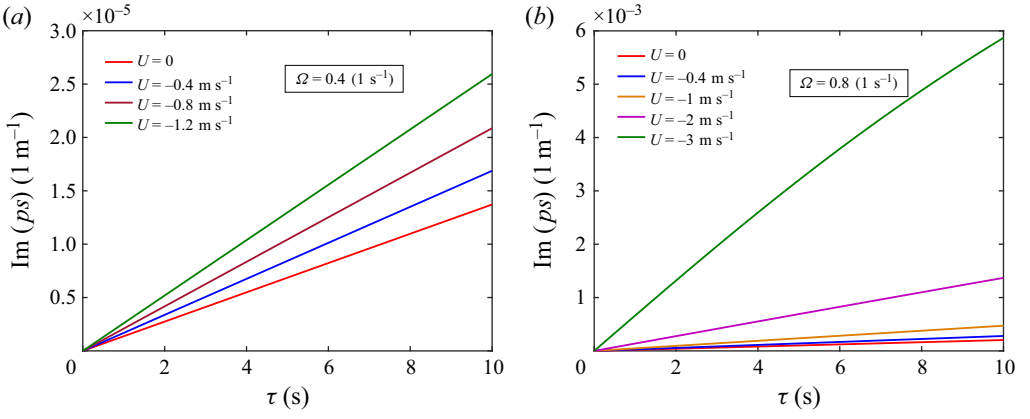


Figure 19. Variations of the imaginary part of the wavenumber, Im (p_S), associated with the plate-covered surface as in (3.15) as a function of τ for different values of upper-layer speed U with stationary lower layer for (a) $\Omega = 0.4\ 1\,s^{-1}$ and (b) $\Omega = 0.8\ 1\,s^{-1}$.

the values of Im (p_S) become higher for higher values of uniform current U, irrespective of the values of τ and Ω. This implies that stronger opposing currents enhance wave decay. A comparison between figures 18(a) and 18(b) highlights that the values of Im (p_S) are significantly higher for $\Omega = 0.8\ 1\,s^{-1}$, compared with $\Omega = 0.4\ 1\,s^{-1}$, regardless of the values of U. This implies that the flexural-gravity wave with a higher frequency is decaying faster than that of the lower-frequency wave. Figure 19 considers a scenario where the upper layer moves with a speed U over a stationary lower layer, in contrast to the uniform current case where both layers move with the same speed U. Figure 19 exhibits the changes in the values of Im (p_S) versus the retardation time τ for $\Omega = 0.4$ and $0.8\ 1\,s^{-1}$. Figure 19 depicts qualitatively similar observations to those shown in figure 18. A comparison of figures 18 and 19 reveals that the values of Im (p_S) become higher for given values of τ when both the upper and lower layers are moving with uniform speed U. This is due to the fact that, when both layers move with uniform speed, the relative velocity between the layers is zero, leading to no shear at the interface.

In figure 20(a), the interfacial wave dispersion curve (3.10) for $\tau = 0$ with opposing uniform current is demonstrated for $U = -0.4\ m\,s^{-1}$. Wave blocking occurs for certain values of frequency Ω and wavenumber p, marked with a green square in figure 20(a) for $\tau = 0$. This observation is similar to that of figure 8(a) for $U = -0.6\ m\,s^{-1}$. On the other hand, the loci of the roots associated with the interfacial wave with opposing uniform current are demonstrated in figure 20(b) for frequencies close to the blocking point, with $0.2 \leqslant \Omega \leqslant 0.3255\ 1\,s^{-1}$, in the presence of retardation times $\tau = 0.1$ s and $\tau = 1$ s. Figure 20(b) reveals that root coalescence, an expected characteristics for the occurrence of wave blocking, does not occur in the presence of retardation time τ. It is observed that the roots of the interfacial wave dispersion relation (3.10) are moving away from each other in the vicinity of the blocking point for $\tau > 0$. Additionally, a significant variation between the loci of the roots is found near the blocking point for $\tau = 1$ s compared with that of $\tau = 0.1$ s, implying that the larger retardation time leads to more pronounced deviations. The values of Im (p) are close to the real axis for frequency, Ω, prior to the occurrence of wave blocking, which implies the existence of two predominant interfacial waves in the downstream direction. Nevertheless, the imaginary component of the roots corresponding to the interfacial wave is $O(10^{-5})$ for $\tau = 1$ s and less for $\tau = 0.1$ s, analogous to the discussions in the case of flexural-gravity waves mentioned in figure 18.

https://doi.org/10.1017/jfm.2025.10268 Published online by Cambridge University Press

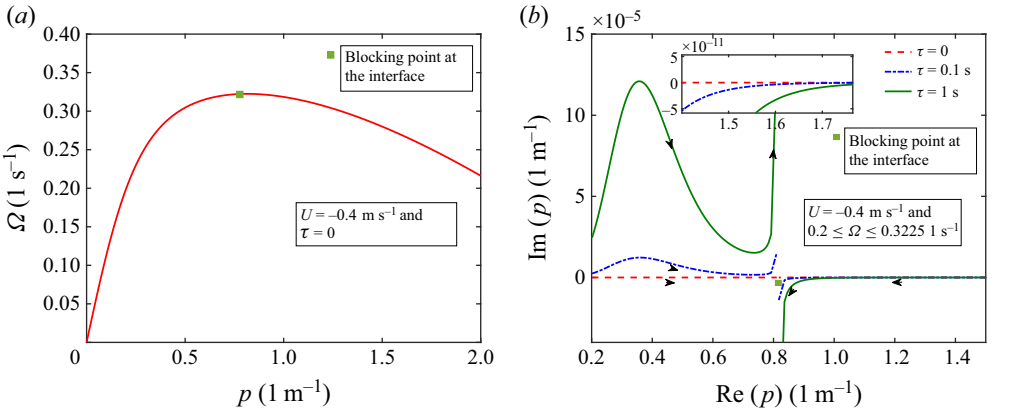


Figure 20. (*a*) Variations of the interfacial wave dispersion curve against the current with $\tau = 0$, and (*b*) loci of the roots for $\tau = 0$, 0.1 and 1 s with frequencies close to the blocking point, within the range $0.2 \leqslant \Omega \leqslant 0.3225$ 1 s^{-1}, considering uniform current $U = -0.4$ m s^{-1} in both the layers and $s = 0.9$.

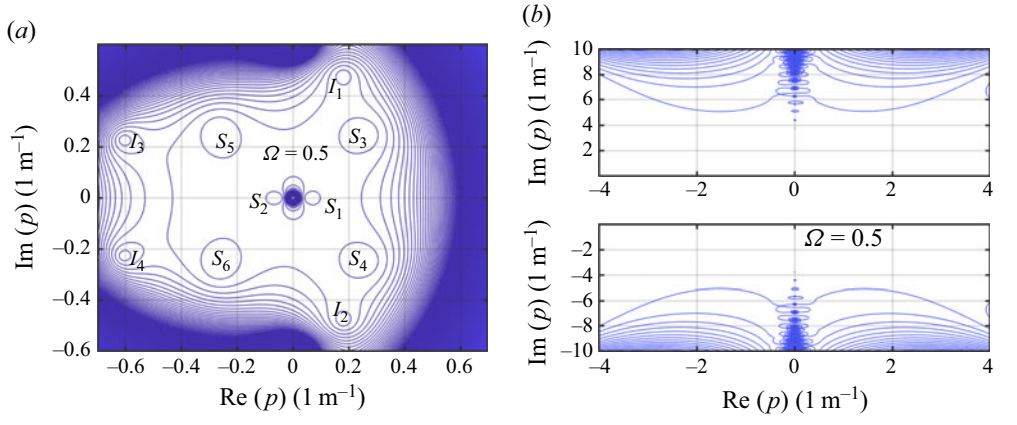


Figure 21. (*a*, *b*) Contour plots of the dispersion relation (3.8) for $U_1 = -1$ m s^{-1}, $U_2 = 0.5$ m s^{-1}, $\Omega = 0.5$ 1 s^{-1} and $\tau = 0.1$ s.

In figure 21, the contour plots of the dispersion relation (3.8) are exhibited for $\Omega = 0.5$ 1 s^{-1} and $\tau = 0.1$ s in the presence of varying currents $U_1 = -1$ m s^{-1} and $U_2 = 0.5$ m s^{-1} in the upper and lower layers, respectively. The six complex roots associated with the flexural-gravity wave are denoted by S_j, $j = 1, 2, 3, 4, 5, 6$, whereas the four roots corresponding to the interfacial wave are shown by I_j, $j = 1, 2, 3, 4$. The roots represent solutions to the dispersion relation that describe wave modes with distinct propagation and decay characteristics. Figure 21(*a*) reveals that the roots at the points S_1 and S_2 are the predominant wave in the plate-covered surface, and the roots at the points I_3 and I_4 are the predominant waves in the interface. The other roots are rapidly decaying waves. Figure 21(*b*) depicts the existence of infinitely many purely imaginary roots of the dispersion relation (3.8). A comparison with the $\tau = 0$ case (see figure 12) reveals a noticeable shift in the positions of the roots when $\tau = 0.01$ s. This shift underscores the influence of the plate's viscoelastic properties and the velocity difference between the layers on the wave dynamics, highlighting their role in modifying the dispersion characteristics.

https://doi.org/10.1017/jfm.2025.10268 Published online by Cambridge University Press

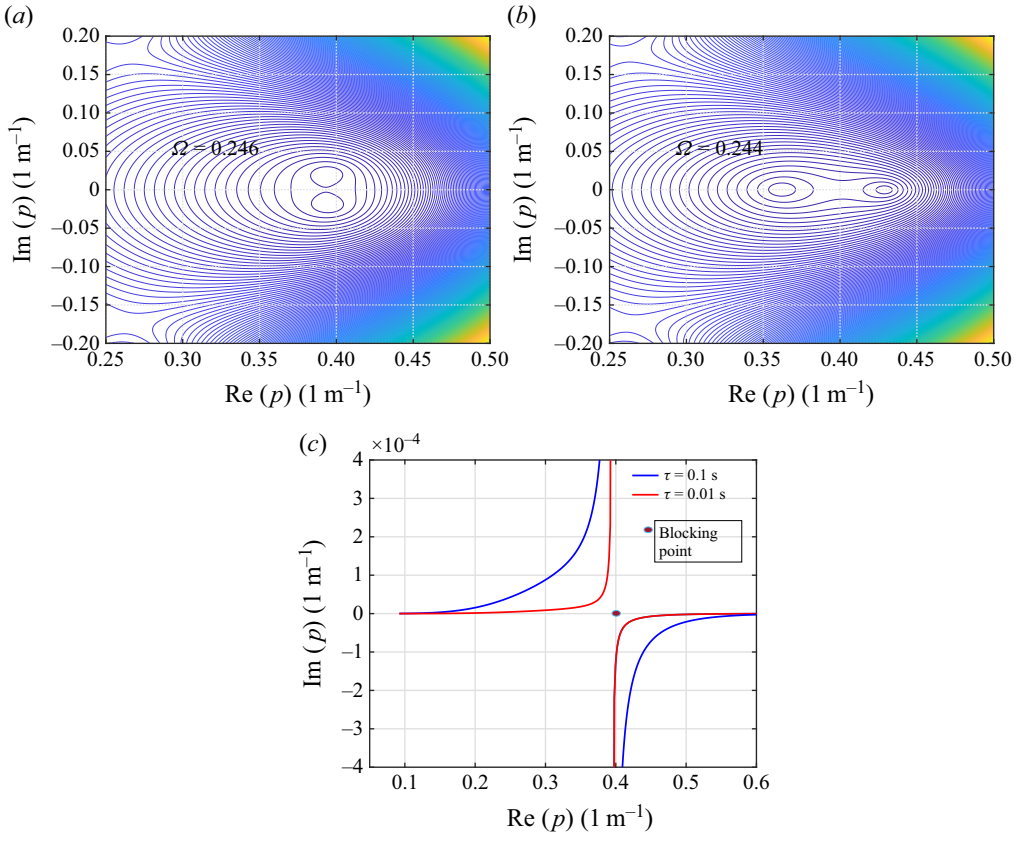


Figure 22. (*a, b*) Change in position of the roots at the points I_1 and I_2 in figure 21 for $\Omega = 0.244\ 1\,s^{-1}$ and $\Omega = 0.246\ 1\,s^{-1}$, and (*c*) loci of the roots at the points $I_j,\ j = 1, 2$ for two different values of τ with frequency within the range $0.2 \leqslant \Omega \leqslant 0.25\ 1\,s^{-1}$. Here, (*a*) and (*b*) are taken as snapshots from a movie file 'Movie 22'.

Figures 22(*a*) and 22(*b*) demonstrate the change in position of the roots at the points I_1 and I_2 for $\Omega = 0.246\ 1\,s^{-1}$ and $\Omega = 0.244\ 1\,s^{-1}$ with other parameters remaining the same as in figure 21. It is observed that the roots at points I_1 and I_2 associated with the interfacial wave approach each other for $\Omega = 0.246\ 1\,s^{-1}$, which corresponds with the blocking point for $\tau = 0$ as shown in figure 12. Moreover, for $\Omega = 0.244\ 1\,s^{-1}$, the two roots become predominant in the interfacial wave propagating with opposing currents. It is pertinent to note that the predominant waves at the points I_1 and I_2 are complex with positive and negative imaginary parts, respectively, for $\tau = 0.1$ s. On the other hand, figure 22(*c*) depicts the loci of the roots at the points I_1 and I_2 for $\tau = 0.1$ and $\tau = 0.01$ with frequency Ω lying in the range $0.2 \leqslant \Omega \leqslant 0.25\ 1\,s^{-1}$. As τ increases, the roots diverge further, reflecting the damping effects introduced by the retardation time. This behaviour is consistent with the observations in figure 20(*b*). However, for any frequency within the primary and secondary blocking points, as mentioned in Sub § 5, three predominant flexural-gravity waves with opposing currents exist. This suggests that multiple predominant waves exist either in the plate-covered surface or in the interface, depending on the values of current speed and frequency irrespective of the presence of plate viscosity.

https://doi.org/10.1017/jfm.2025.10268 Published online by Cambridge University Press

7. Flexural-gravity analogue of dead water

Here, the amplitude ratio (3.7) is examined for various parameter values in the reference cases: uniform current U in each layer and the upper layer is moving with speed U_1 over a stationary lower layer. In this subsection, a physical phenomenon, namely the dead-water analogue (see Das *et al.* 2018*c*; Boral *et al.* 2022) of a flexural-gravity wave in a two-layer density-stratified fluid having a viscoelastic plate-covered surface and a free interface is analysed.

Equation (3.7) reveals that

$$\left|\frac{\eta_{20}}{\eta_{10}}\right| \to \infty \qquad \text{as } s \to 1, \tag{7.1}$$

for wavenumber p, corresponds with the interfacial wave for a given frequency Ω. Equation (7.1) signifies that the amplitude of the flexural-gravity wave diminishes significantly when the densities of the two fluids become close to each other. The parameters are considered the same as in § 5, unless otherwise specified. Note that certain values of flow speed in each of the upper and lower layers are considered for clarity when investigating the physical phenomenon. However, this section can also be applied to other parameters as needed.

Figure 23 demonstrates the variations in the absolute values of the amplitude ratio of interfacial wave amplitude to that of the deflection of a floating viscoelastic plate, $|\eta_{20}/\eta_{10}|$, as a function of density ratio s for different values of frequency Ω, retardation time τ and uniform current U in each of the upper and lower layers. This ratio exhibits the relationship between the amplitude of the interfacial wave at the interface of the fluid layers and the deflection of the floating plate on the surface, showing how the two are influenced by the flow and wave dynamics. Figure 23(*a*) depicts that the values of the amplitude ratio $|\eta_{20}/\eta_{10}|$ increases with an increase in the values of frequency Ω, which implies that the energy associated with the interfacial wave becomes more dominant relative to the surface deflection as the frequency increases. Additionally, there is a negligible variation in the values of amplitude ratio, $|\eta_{20}/\eta_{10}|$, for $\tau = 0$ and $\tau = 1$ s, highlighting that the retardation time has a limited influence on the interaction of predominant waves at the interface. This is because the imaginary component of the predominant wave corresponding to the interface is very small for $\tau > 0$, as shown in figure 20(*b*). In figure 23(*b*), the absolute values of the amplitude ratio, $|\eta_{20}/\eta_{10}|$, are illustrated for interfacial waves with opposing current and following current for $U = -0.2$ m s^{-1}, $\Omega = 0.4$ 1 s^{-1} and $\tau = 1$ s. It is observed that the amplitude ratio, $|\eta_{20}/\eta_{10}|$, for both the interfacial waves in the direction of current and the opposite direction of current are similar for the density ratio $s \leqslant 0.8$. However, for $s > 0.8$, the amplitude ratio becomes higher for the interfacial wave with opposing current than that of the interfacial wave with following current. This is attributed to higher values of the real part of the wavenumber, Re (p_I), associated with the interfacial wave in the opposite direction of current than that in the direction of current for $\tau = 1$ s, as shown in figure 23(*c*). Note that a higher wavenumber indicates shorter wavelengths and potentially more pronounced wave behaviour in the opposing current scenario, leading to a higher amplitude ratio.

In figure 24, absolute values of the amplitude ratio $|\eta_{20}/\eta_{10}|$ versus density ratio s are demonstrated in a two-layer density-stratified fluid where the upper layer is moving with a certain speed, U_1, over a stationary lower layer. Here, two different cases, $U_1 = -0.2$ m s^{-1} with $\Omega = 0.4$ 1 s^{-1} in figure 24(*a*), and $U_1 = -0.6$ m s^{-1} with $\Omega = 0.2$ 1 s^{-1} in figure 24(*b*) are considered in the presence of retardation time $\tau = 1$ s. Figure 24(*a*) illustrates a qualitatively similar observation to that of figure 23(*a*). A comparison of

https://doi.org/10.1017/jfm.2025.10268 Published online by Cambridge University Press

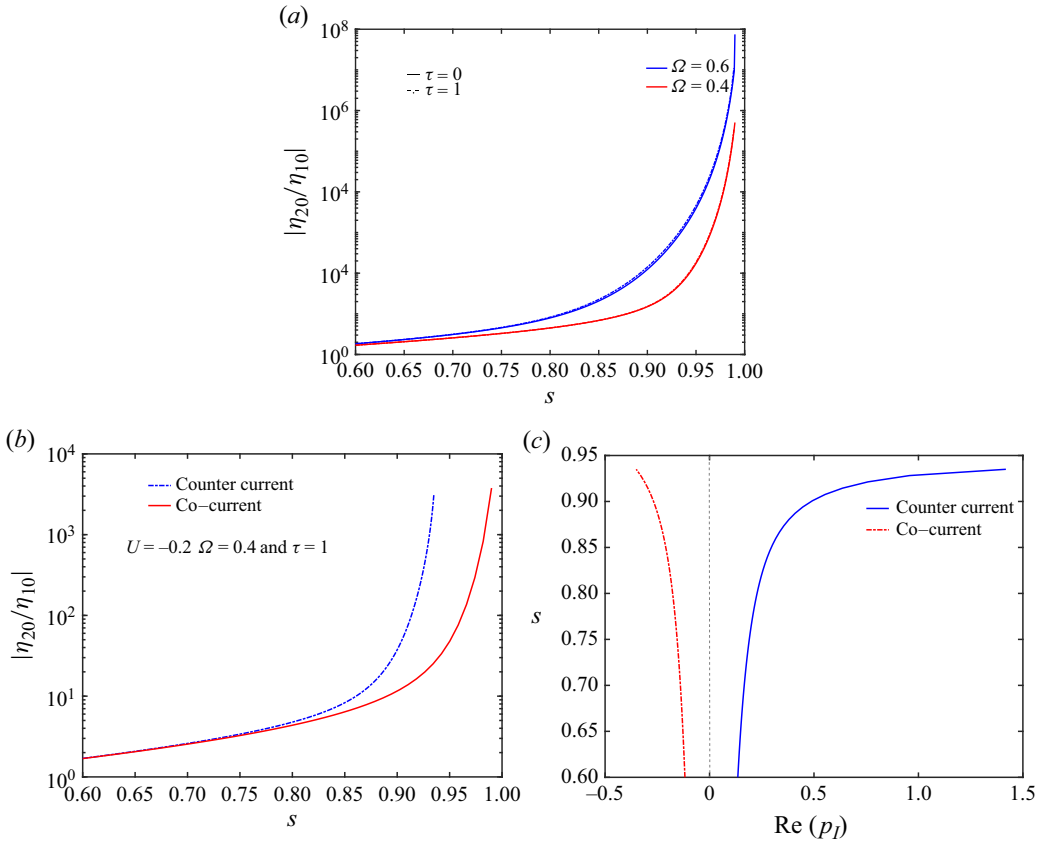


Figure 23. Variations in the absolute values of amplitude ratio $|\eta_{20}/\eta_{10}|$ versus density ratio s for (*a*) $U = 0$ and (*b*) $U = -0.2\ \mathrm{m\,s^{-1}}$ in each layer with frequency Ω in the presence of retardation time τ. (*c*) Changes in the real part of the wavenumber associated with the interfacial wave, Re (p_I), versus density ratio s.

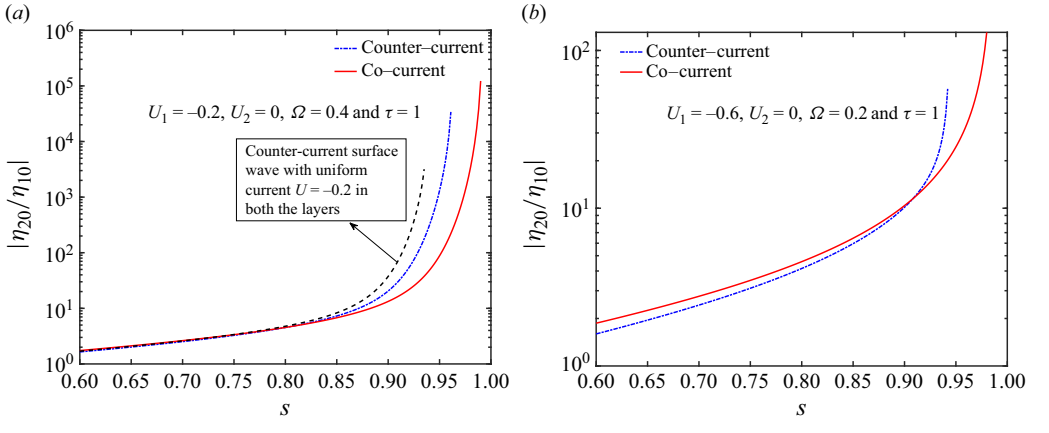


Figure 24. Variations in the amplitude ratio $|\eta_{20}/\eta_{10}|$ versus density ratio s for a moving upper layer with speed U_1 and frequency Ω are shown in (*a*) $U_1 = -0.2\ \mathrm{m\,s^{-1}}$, $\Omega = 0.4\ 1\ \mathrm{s^{-1}}$ and (*b*) $U_1 = -0.6\ \mathrm{m\,s^{-1}}$, $\Omega = 0.2\ 1\ \mathrm{s^{-1}}$ with $\tau = 1$ s.

https://doi.org/10.1017/jfm.2025.10268 Published online by Cambridge University Press

figures 24(*a*) and 23(*b*) exhibits that the amplitude ratio, $|\eta_{20}/\eta_{10}|$, is higher for $s > 0.8$ when the upper layer is moving with a certain speed over a stationary lower layer. Figure 24(*b*) reveals that the values of $|\eta_{20}/\eta_{10}|$ are higher for the interfacial waves propagating in the direction of upper-layer velocity U_1 than those of the interfacial wave in the opposite direction to U_1 for $s < 0.92$. On the contrary, an opposite phenomenon occurs for $s > 0.92$. Figures 23 and 24 conclude that the deflection of the floating viscoelastic plate is reduced significantly when the densities of the upper- and lower-layer fluids close to each other regardless of frequency, Ω, and upper- and lower-layer velocities U_j.

8. Conclusion

The interaction between flexural-gravity waves and interfacial waves in a two-layer density-stratified fluid with a tangential discontinuity of velocity across the interface was investigated using a two-dimensional linear wave theory and small-amplitude structural responses. The presence of different current speed in the upper and lower layers gives rise to phenomena such as wave blocking and KH instability, both of which were explored in detail. The floating plate was modelled using the KV model, which introduced viscous damping into the structural analysis via a retardation time. A dispersion relation was derived for flexural-gravity waves in a two-layer fluid with a viscoelastic plate-covered surface and free interface and different current speeds in the upper and lower layers.

This work revealed that the dispersion relation possesses four complex roots for any real wavenumber and other given parameters of the problem in the presence of the retardation time. To provide further insight, the dispersion relation was simplified for two reference cases: uniform current and a moving upper layer over a stationary lower layer. Separate investigations were conducted on short flexural-gravity waves and interfacial waves to better understand the criteria for wave blocking and KH instability in the absence of a retardation time. Critical values of current speeds and wavenumbers, where wave blocking occurs for either type of wave, were determined and analysed. Additionally, the onset of KH instability in short interfacial waves was studied in connection with wave blocking, showing that wave blocking precedes instability.

The present work demonstrated that the occurrence of wave blocking in flexural-gravity waves, without a retardation time, depends on the depths of the upper- and lower-layer fluids. Additionally, it was found that the frequency beyond which interfacial waves do not propagate in the opposite direction to the current reduces as the depths of the upper and lower layers are reduced. Moreover, no wave blocking occurs in either the floating elastic plate-covered surface or the interface when waves propagate in the direction of the current. Wave blocking did not occur simultaneously in the plate-covered surface and interface for any values of uniform current and frequency. The study suggested that multiple waves can propagate either on the interface or on the elastic plate-covered surface in the direction opposite to the current, depending on the values of current speed and frequency prior to the blocking point. On the other hand, KH instability occurs in the interfacial wave, which propagates in the direction of the upper-layer velocity when the lower layer moves at a speed different from the upper layer. It was observed that interfacial wave blocking occurs before the occurrence of KH instability in finite water depth. The wavelength and phase speed of the interfacial wave in the opposite direction to the upper-layer velocity are reduced when the upper and lower layers move in the same direction compared with when they move in opposite directions at the same speed. It was found that the flexural-gravity waves in the following and opposing directions of the upper-layer velocity are not influenced by the change in the direction of the lower-layer velocity. However, the values of frequency and wavenumber at which KH instability occurs

https://doi.org/10.1017/jfm.2025.10268 Published online by Cambridge University Press

in the interfacial wave are reduced to smaller values when the lower layer moves in the opposite direction to the upper layer with the same speed. The real roots of the dispersion relation become complex with small imaginary parts if small retardation time is included. These roots are associated with so-called predominant waves. The study explored that the real component of the frequency of temporally damped flexural-gravity waves possesses a maximum and decreases for higher values of wavenumber. For spatially damped waves, the study revealed that the complex roots of the dispersion relation do not coalesce in the vicinity of blocking points in the presence of the retardation time. However, more than one predominant wave exists either in the viscoelastic plate-covered surface or in the interface, depending on the values of frequency, current velocity in the upper and lower layers and other parameters. This was demonstrated through contour plots of the dispersion relation for frequencies close to the blocking points. Moreover, a video file is attached as a supplementary document for better visualisation of the loci of the roots near the blocking point in the presence of a plate viscosity. We acknowledge that a rigorous derivation of the complex group velocity for flexural-gravity waves with a plate viscosity would be a valuable theoretical contribution. However, such an analysis requires a more detailed mathematical framework and is beyond the scope of the present study, which is focused primarily on the linear dispersive behaviour and damping characteristics of flexural-gravity and interfacial waves. We have suggested it as a natural and important direction for future research. Furthermore, the study depicted that the flexural-gravity wave amplitude approaches zero, whilst the interfacial wave amplitude remains small when the densities of the upper and lower layers are close to each other. Note that the present study is based on linear theory of water waves, while the study of nonlinear wave systems in a two-layer fluid with a discontinuous mean flow is indeed a distinct area and an important direction for future research.

Supplementary movies. Supplementary movies are available at https://doi.org/10.1017/jfm.2025.10268.

Funding. This work is supported by the National Natural Science Foundation of China (Nos. W2433140, 52192693, 52192690, 52371270, U20A20327, 52350410468), for which B.-Y. N. and S. B. are most grateful.

Declaration of interests. The authors report no conflict of interest.

References

ALAM, M.R., LIU, Y. & YUE, D.K.P. 2009*a* Bragg resonance of waves in a two-layer fluid propagating over bottom ripples. Part I. Perturbation analysis. *J. Fluid Mech.* **624**, 191–224.

ALAM, M.R., LIU, Y. & YUE, D.K.P. 2009*b* Bragg resonance of waves in a two-layer fluid propagating over bottom ripples. part ii. Numerical simulation. *J. Fluid Mech.* **624**, 225–253.

BARMAN, S.C., BORAL, S. & SAHOO, T. 2023 Bragg scattering of flexural-gravity waves by a series of polynyas in the context of blocking dynamics. *Phy. Fluids* **35** (1), 016601.

BEBIEVA, Y. & TIMMERMANS, M.-L. 2019 Double-diffusive layering in the Canada basin: an explanation of along-layer temperature and salinity gradients. *J. Geophys. Res.: Oceans* **124** (1), 723–735.

BISHT, N., BORAL, S., SAHOO, T. & MEYLAN, M.H. 2023 Triad resonance of flexural gravity waves in the presence of shear current with constant vorticity. *Phy. Fluids* **35** (11), 116605.

BONTOZOGLOU, V. & HANRATTY, T.J. 1988 Effects of finite depth and current velocity on large amplitude Kelvin–Helmholtz waves. *J. Fluid Mech.* **196**, 187–204.

BORAL, S., BARMAN, S.C. & SAHOO, T. 2023*a* *Wave Scattering by an Array of Moored Floating Flexible Plates Resting On an Elastic Foundation in the Reference of Blocking Dynamics*. Waves Random Complex Media.

BORAL, S., DAS, S., SAHOO, T. & MEYLAN, M.H. 2022 Blocking dynamics of capillary-gravity waves in a two-layer fluid in the presence of surface and interfacial tensions. *Meccanica* **57** (6), 1307–1335.

BORAL, S., MEYLAN, M.H., SAHOO, T. & NI, B.-Y. 2023*b* Time-dependent flexural gravity wave scattering due to uneven bottom in the paradigm of blocking dynamics. *Phys. Fluids* **35** (11), 116603.

https://doi.org/10.1017/jfm.2025.10268 Published online by Cambridge University Press

BORAL, S., NATH, S., SAHOO, T. & MEYLAN, M.H. 2021*a* The role of viscoelastic foundation on flexural gravity wave blocking in shallow water. *AIP Adv.* **11** (6), 065317.
BORAL, S. & NI, B.-Y. 2025 Dynamic response of a floating flexible plate to a localised time-periodic and moving load. *Appl. Math. Model.* **143**, 115993.
BORAL, S., SAHOO, T. & STEPANYANTS, Y. 2021*b* Modulation instability of hydro-elastic waves blown by a wind with a uniform vertical profile. *Fluids* **6** (12), 458.
CAIRNS, R.A. 1979 The role of negative energy waves in some instabilities of parallel flows. *J. Fluid Mech.* **92** (1), 1–14.
CARR, M., *et al.* 2019 Laboratory experiments on internal solitary waves in. *Geophys. Res. Lett.* **46** (21), 12230–12238.
CHAWLA, A. & KIRBY, J.T. 1999 Experimental study of wave breaking and blocking on opposing currents. In *Coast. Eng. Conf., Copenhagen, Denmark, 22-26 June*, vol. 1, pp. 759-759–772. ASCE.
CHAWLA, A. & KIRBY, J.T. 2002 Monochromatic and random wave breaking at blocking points. *J. Geophys. Res.: Oceans* **107** (C7), 4–1.
CUSHMAN-ROISIN, B. 2005 Kelvin–Helmholtz instability as a boundary-value problem. *Environ. Fluid Mech.* **5** (6), 507–525.
CZIPOTT, P.V., LEVINE, M.D., PAULSON, C.A., MENEMENLIS, D., FARMER, D.M. & WILLIAMS, R.G. 1991 Ice flexure forced by internal wave packets in the arctic ocean. *Science* **254** (5033), 832–835.
DAS, S., KAR, P., SAHOO, T. & MEYLAN, M.H. 2018*a* Flexural-gravity wave motion in the presence of shear current: Wave blocking and negative energy waves. *Phys. Fluids* **30** (10), 106606.
DAS, S., SAHOO, T. & MEYLAN, M.H. 2018*b* Dynamics of flexural gravity waves: from sea ice to Hawking radiation and analogue gravity. *Proc. R. Soc. Lond. A: Math. Phys. Engng Sci.* **474** (2209), 20170223.
DAS, S., SAHOO, T. & MEYLAN, M.H. 2018*c* Flexural-gravity wave dynamics in two-layer fluid: blocking and dead water analogue. *J. Fluid Mech.* **854**, 121–145.
DAVYS, J.W., HOSKING, R.J. & SNEYD, A.D. 1985 Waves due to a steadily moving source on a floating ice plate. *J. Fluid Mech.* **158**, 269–287.
DINGEMANS, W.M. 1997 *Water Wave Propagation over Uneven Bottoms (in 2 Parts)*, vol. 13. world Scientific.
DUFFY, D.G. 1991 The response of floating ice to a moving, vibrating load. *Cold Reg. Sci. Technol.* **20** (1), 51–64.
DUFFY, D.G. 1996 On the generation of internal waves beneath sea ice by a moving load. *Cold Reg. Sci. Technol.* **24** (1), 29–39.
EKMAN, V.W. 1904 On dead water. *Sci. Results Norw. Polar Expedi.* **5** (15), 152.
FABRIKANT, A.L. & STEPANYANTS, Y.A. 1998 *Propagation of Waves in Shear Flows*, vol. 18. World Scientific Publishing Company.
FOX, W.L. 2011 *Terra Antarctica: Looking into the Emptiest Continent*. Trinity University Press.
GERASIK, V. & STASTNA, M. 2010 Complex group velocity and energy transport in absorbing media. *Phys. Rev. E* **81** (5), 056602.
GREENHILL, A.G. 1886 Wave motion in hydrodynamics. *Am. J. Maths* **9** (1), 62–96.
GRUE, J., BOURGAULT, D. & GALBRAITH, P.S. 2016 Supercritical dead water: effect of nonlinearity and comparison with observations. *J. Fluid Mech.* **803**, 436–465.
HAO, X. & SHEN, L. 2020 Direct simulation of surface roughness signature of internal wave with deterministic energy-conservative model. *J. Fluid Mech.* **891**, R3.
HOSKING, R.J., SNEYD, A.D. & WAUGH, D.W. 1988 Viscoelastic response of a floating ice plate to a steadily moving load. *J. Fluid Mech.* **196**, 409–430.
KHABAKHPASHEVA, T. & KOROBKIN, A.A. 2021 Blunt body impact onto viscoelastic floating ice plate with a soft layer on its upper surface. *Phys. Fluids* **33**, 062105.
KHEISIN, D.E. 1963 Movement of a loading over an elastic plate, floating on the surface of an ideal liquid. Izv. Akad. Nauk SSSR, Otd. Tekh. Nauk 1.
KOZIN, V.M. & POGORELOVA, A.V. 2009 Effect of the viscosity properties of ICE on the deflection of an ICE sheet subjected to a moving load. *J. Appl. Mech. Tech. Phys.* **50** (3), 484–492.
KUNDU, P.K., COHEN, I.M. & DOWLING, D.R. 2015 *Fluid Mechanics*. Academic press.
LAKES, R.S. 2017 *Viscoelastic Solids (1998)*. CRC press.
LAMAS-PARDO, M., IGLESIAS, G. & CARRAL, L. 2015 A review of very large floating structures (VLFS) for coastal and offshore uses. *Ocean Engng* **109**, 677–690.
LIN, S. 2021 Study of wave-current-ice interactions over the northwest atlantic. PhD thesis, Dalhousie University, 273 pp.
MAÏSSA, P., ROUSSEAUX, G. & STEPANYANTS, Y. 2016 Wave blocking phenomenon of surface waves on a shear flow with a constant vorticity. *Phys. Fluids* (1994-present) **28**, 032102.

https://doi.org/10.1017/jfm.2025.10268 Published online by Cambridge University Press

MARTIN, C.-I. & PĂRĂU, E.I. 2025 Hamiltonian formulation for interfacial periodic waves propagating under an elastic sheet above stratified piecewise constant rotational flow. *Wave Motion* **133**, 103454.
MATIUSHINA, A.A., POGORELOVA, A.V. & KOZIN, V.M. 2016 Effect of impact load on the ice cover during the landing of an airplane. *Intl J. Offshore Polar Engng* **26** (01), 6–12.
MIKAELYAN, M.A. 2017 On the energy transport velocity in a dissipative medium. *Bull. Lebedev Phys. Inst.* **44** (3), 81–88.
MOHANTY, S.K., MONDAL, R. & SAHOO, T. 2014 Time dependent flexural gravity waves in the presence of current. *J. Fluids Struct.* **45**, 28–49.
NEGI, P., BORAL, S. & SAHOO, T. 2022 Scattering of oblique waves by a semi-infinite floating elastic plate within the framework of wave blocking. *J. Engng Math.* **135** (1), 1.
NEVEL, D.E. 1970 *Moving Loads On a Floating Ice Sheet*, vol. 261. Corps of Engineers, US Army Cold Regions Research & Engineering Laboratory.
PĂRĂU, E.I. 2018 Solitary interfacial hydroelastic waves. *Phil. Trans. R. Soc. A: Math. Phys. Engng Sci.* **376** (2111), 20170099.
PEAKE, N. 2001 Nonlinear stability of a fluid-loaded elastic plate with mean flow. *J. Fluid Mech.* **434**, 101–118.
PEAKE, N. 2004 On the unsteady motion of a long fluid-loaded elastic plate with mean flow. *J. Fluid Mech.* **507**, 335–366.
RIS, R.C. & HOLTHUIJSEN, L.H. 1996 Spectral modelling of current induced wave-blocking. *Coast. Engng* **1996**, 1247–1254.
SCHULKES, R.M., HOSKING, R.J. & SNEYD, A.D. 1987 Waves due to a steadily moving source on a floating ice plate. Part 2. *J. Fluid Mech.* **180**, 297–318.
SHISHMAREV, K., KHABAKHPASHEVA, T. & KOROBKIN, A. 2016 The response of ice cover to a load moving along a frozen channel. *Appl. Ocean Res.* **59**, 313–326.
SMITH, R. 1975 The reflection of short gravity waves on a non-uniform current. *Math. Proc. Camb. Phil. Soc.* **78**, 517–525.
SQUIRE, V.A. 2020 Ocean wave interactions with sea ice: a reappraisal. *Annu. Rev. Fluid Mech.* **52** (1), 37–60.
SQUIRE, V.A., HOSKING, R.J., KERR, A.D. & LANGHORNE, P.J. 2012 *Moving Loads On Ice Plates*, vol. 45. Springer Science & Business Media.
STEPANYANTS, Y.A. & STUROVA, I.V. 2021 Waves on a compressed floating ice plate caused by motion of a dipole in water. *J. Fluid Mech.* **907**, A7.
STOKES, G.G. 1847 On the theory of oscillatory waves. *Trans. Camb. Phil. Soc.* **8**, 441–455.
STUROVA, I.V. 2011 Hydrodynamic loads acting on an oscillating cylinder submerged in a stratified fluid with ice cover. *J. Appl. Mech. Tech. Phys.* **52** (3), 415–426.
TABATA, S. 1958 Heat budget of the water in the vicinity of triple Island, British Columbia. *J. Fish. Res. Board Can.* **15** (3), 429–451.
TAKIZAWA, T. 1985 Deflection of a floating sea ice sheet induced by a moving load. *Cold Reg. Sci. Technol.* **11** (2), 171–180.
TAVAKOLI, S. & BABANIN, A.V. 2023 A collection of wet beam models for wave–ice interaction. *The Cryosphere* **17** (2), 939–958.
TKACHEVA, L.A. 2024 Motion of a load on an ice cover in the presence of a liquid layer with shear current. *Fluid Dyn.* **59** (1), 98–110.
TRULSEN, K. & MEI, C.C. 1993 Double reflection of capillary/gravity waves by a non-uniform current: a boundary-layer theory. *J. Fluid Mech.* **251**, 239–271.
TULIN, M.P. & ZILMAN, G. 1993 Dead-water effects of a ship moving in stratified seas. *J. Offshore Mech. Arctic Eng.* **115**, 105.
WANG, Z., PĂRĂU, E.I., MILEWSKI, P.A. & VANDEN-BROECK, J.-M. 2014 Numerical study of interfacial solitary waves propagating under an elastic sheet. *Proc. R. Soc. Lond. A: Math. Phys. Engng Sci.* **470** (2168), 20140111.
ZENG, L.D., KOROBKIN, A.A., NI, B.-Y. & XUE, Y.Z. 2021 Flexural-gravity waves in ice channel with a lead. *J. Fluid Mech.* **921**, A10.
ZENG, L.D., KOROBKIN, A.A., NI, B.-Y. & XUE, Y.Z. 2022 Moving load in an ice channel with a crack. *Appl. Ocean Res.* **121**, 103086.

https://doi.org/10.1017/jfm.2025.10268 Published online by Cambridge University Press